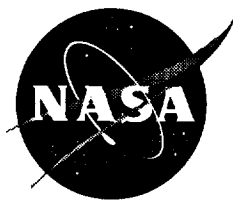NASA/TP-1998-206553

Reynolds Number Effects at High Angles of Attack

*David F. Fisher, Brent R. Cobleigh,
and Daniel W. Banks*
Dryden Flight Research Center
Edwards, California

Robert M. Hall and Richard W. Wahls
NASA Langley Research Center
Hampton, Virginia

June 1998

Available from the following:

REYNOLDS NUMBER EFFECTS AT HIGH ANGLES OF ATTACK

David F. Fisher[*], Brent R. Cobleigh[†], and Daniel W. Banks[‡]
NASA Dryden Flight Research Center, Edwards, California

Robert M. Hall[§] and Richard A. Wahls[#]
NASA Langley Research Center, Hampton, Virginia

Abstract

Lessons learned from comparisons between ground-based tests and flight measurements for the high-angle-of-attack programs on the F-18 High Alpha Research Vehicle (HARV), the X-29 forward-swept wing aircraft, and the X-31 enhanced fighter maneuverability aircraft are presented. On all three vehicles, Reynolds number effects were evident on the forebodies at high angles of attack. The correlation between flight and wind tunnel forebody pressure distributions for the F-18 HARV were improved by using twin longitudinal grit strips on the forebody of the wind-tunnel model. Pressure distributions obtained on the X-29 wind-tunnel model at flight Reynolds numbers showed excellent correlation with the flight data up to $\alpha = 50°$. Above $\alpha = 50°$ the pressure distributions for both flight and wind tunnel became asymmetric and showed poorer agreement, possibly because of the different surface finish of the model and aircraft. The detrimental effect of a very sharp nose apex was demonstrated on the X-31 aircraft. Grit strips on the forebody of the X-31 reduced the randomness but increased the magnitude of the asymmetry. Nose strakes were required to reduce the forebody yawing moment asymmetries and the grit strips on the flight test noseboom improved the aircraft handling qualities.

Nomenclature

BART	Basic Aerodynamics Research Tunnel, Langley Research Center (Hampton, Virginia)
c_y	sectional side force coefficient
C_D	drag coefficient
C_l	rolling moment coefficient
C_{l_β}	dihedral effect, $\partial C_l / \partial \beta$, per deg
C_{n_0}	yawing moment coefficient at $\beta = 0°$
C_{n_0}, fb	forebody yawing moment coefficient
C_{n_β}	static direction stability parameter, $\partial C_n / \partial \beta$, per deg
C_{n_β}, dyn	dynamic directional stability parameter, $C_{n_\beta} \cos\alpha - [I_{ZZ}/I_{XX}] C_{l_\beta} \sin\alpha$
C_{N_0}	normal force coefficient at $\beta = 0°$
C_p	pressure coefficient
C_{Y_0}	side force coefficient at $\beta = 0°$
C_{Y_0}, max	maximum overall side force coefficient for all roll orientations at $\beta = 0°$
D	base diameter of forebody, in.
DARPA	Defense Advanced Research Projects Agency
DTRC	David Taylor Research Center, Bethesda, Maryland
EFM	enhanced fighter maneuverability
FSW	forward-swept wing
F.S.	fuselage station, in.
g	gravity force
HARV	High Alpha Research Vehicle
HST	High Speed Tunnel, Langley Research Center (Hampton, Virginia)
I_{XX}, I_{ZZ}	moments of inertia about the X and Z body axis, respectively, slug-ft^2
l	fuselage or body length, in.
l_n	nose length, in.

LEX	leading edge extensions
LTPT	Low-Turbulence Pressure Tunnel, Langley Research Center
M	Mach number
McAir LSWT	McDonnell-Douglas, (now Boeing), St. Louis Low-Speed Wind Tunnel
NTF	National Transonic Facility, Langley Research Center (Hampton, Virginia)
q	dynamic pressure, lb/ft^2
r	nose radius, in.
Re_c	Reynolds number based on mean aerodynamic chord
Re_D	Reynolds number based on forebody base diameter
Re_d	Reynolds number based on noseboom or cylinder diameter
x	axial distance from nose tip, in.
α	angle of attack, deg
β	angle of sideslip, deg
θ	circumferential angle, deg
ϕ	roll angle, deg

Introduction

Over the past 10 years, three high angle of attack research programs were flown at the NASA Dryden Flight Research Center, Edwards, California. These programs included the F-18 High Alpha Research Vehicle (HARV) (fig. 1), the X-29A forward-swept wing (FSW) airplane (fig. 2), and the X-31 enhanced fighter maneuverability (EFM) airplane (fig. 3). The flight tests were complemented with ground tests in wind tunnels, primarily at the Langley Research Center, Hampton, Virginia. Limited water tunnel flow visualization tests were performed at Dryden Flight Research Center. Many of the results obtained from these programs can be found in a series of High-Angle-of-Attack Technology Conference Proceedings.[1, 2, 3, 4]

The F-18 HARV was a highly instrumented pre-production F/A-18A aircraft. All four NASA aeronautical centers (Ames, Dryden, Langley, and Lewis) worked closely together on the HARV program. The flight program had three distinct phases. In phase one, the airplane was flown in the basic fighter escort configuration and collected aerodynamic and flow

visualization data. For phase two, thrust-vectoring paddles were installed on the airplane at the exhaust exit. During this second phase, research was emphasized in flight controls, handling qualities, agility and propulsion. For phase three, a new radome with actuated nose strakes was built and installed on the aircraft to enhance fighter agility. The research emphasis during this third phase was on aerodynamics, flow visualization, controls, handling qualities and agility.

Two airplanes were designed and built by Grumman Aerospace Corporation (Bethpage, New York) for the joint Air Force-NASA X-29A forward-swept wing airplane program. The major players in this program were the Defense Advanced Research Projects Agency (DARPA), the Air Force Wright Aeronautical Laboratory and Flight Test Center, the NASA Langley Research Center and Dryden Flight Research Center, and the Grumman Aerospace Corporation. Only one aircraft, ship 2, was equipped with a spin chute and flown at high angles of attack. Data were obtained to support aerodynamics, flow visualization, controls, handling qualities, and agility research during the high angle of attack portion of the program.

Two X-31 aircraft were jointly designed and built by the North American Division of Rockwell International (Downey, California) and Deutsche Aerospace (DASA) (Munich, Germany). This program was run by an International Test Organization comprised of DARPA, the U.S. Navy, the U.S. Air Force, Rockwell International, DASA, and NASA. The goals of the flight program were to demonstrate EFM technologies, investigate close-in-combat exchange ratios, develop design requirements, build a database for application to future fighter aircraft, and develop and validate low-cost prototype concepts. The X-31 instrumentation system did not measure local surface pressures; however, the detailed envelope expansion captured a large amount of static and dynamic force and moment data.

This paper presents the Reynolds number effects that were observed during the ground and flight testing of the F-18 HARV, the X-29 FSW, and X-31 EFM airplanes at high angles of attack. These discussions are primarily limited to the forebody effects. Suggestions to improve the ground-test-to-flight correlations are offered. Warnings that indicate where caution is needed when extrapolating low Reynolds number data to flight Reynolds number data are also given.

Background

Most modern fighter aircraft of today, such as the F-14, F-15, F-16, and F/A-18, have long slender forebodies. This is also true of the three test aircraft discussed in this paper, the F-18 HARV, the X-29, and the X-31.

Slender bodies have been studied extensively in ground facilities at high angles of attack and Reynolds number effects have been identified. Lamont[5] conducted a test on an ogive cylinder over a wide range of angles of attack and Reynolds numbers that showed a strong correlation of Reynolds number and boundary-layer state with the maximum overall side force. Shown in figure 4,[5] large side forces can be generated at high angles of attack for zero sideslip and these side forces can vary significantly depending upon the Reynolds number. As shown in figure 5 for $\alpha = 55°$,[5] the maximum overall side force is greatest for both laminar and fully turbulent separation, and is smallest for transitional boundary layer separation. Note the sharp changes in side force for small Reynolds number changes. For an aircraft flying at high angle of attack and high altitude, the flying qualities might be good where the forebody boundary layer separation is in the transitional range. However, at a lower altitude, the same aircraft at the same angle of attack and Mach number may experience a much higher, and perhaps unexpected, yawing moment because of turbulent boundary layer separation.

Hall[6] analyzed the Lamont data further in detail and included the flow visualization results of Keener[7] for a similar tangent-ogive. In figure 6,[6] the sectional side force is shown as a function of x/D for Reynolds numbers in the laminar, transitional and turbulent boundary layers separation states. Notice that the laminar and transitional cases have their maximum sectional side force near the apex, whereas for the turbulent case, two sectional side force peaks are present, one at $x/D = 2$ and another at $x/D = 4.5$. Because of this effect, Hall warns of extrapolating laminar or transitional yawing moment data to higher values of Reynolds numbers. Unfortunately, much of the wind tunnel data at high angles of attack is taken in the laminar or transitional Reynolds number range based on forebody diameter.

Small, undetectable asymmetries in the nose shape can also cause sharp changes in side force. In figure 7,[5] the overall side and normal force are shown as a function of roll angle at $\alpha = 55°$ and $Re_D = 3 \times 10^6$. As the ogive-cylinder was rotated, the side force switched from a maximum side force to the right to a maximum side

force to the left in 20° to 30° of rotation. The effect of roll angle on normal force coefficient is much less. This example shows how rapidly an asymmetry in one direction can switch to an asymmetry in the opposite direction. Changes in the boundary-layer state can cause an effect similar to the undetectable asymmetric effects. In flight, it is difficult to tell the difference between the two effects because the result may be the same.

The effect of nose bluntness on side force coefficient is shown from Hunt[8] (fig. 8). This figure shows that blunting the nose (increasing the nose radius) can have the favorable effect of reducing the side force significantly. In figure 9, Chapman[9] shows the wide range in angle of attack, $40° \leq \alpha \leq 70°$ over which asymmetries act on a sharp tangent ogive. A reversal of side force is also shown in the same angle of attack range. The beneficial effect of blunting can also be seen in this figure. However, note the Reynolds number based on forebody diameter at which the data from the last two figures were obtained. One case, in figure 8, was in the laminar boundary layer separation range while the rest of the data in figure 8 and figure 9 were in the transitional range, exactly where the data from Lamont (fig. 5) showed the smallest side force. Keener[10] tested a 3.5 tangent-ogive with a nose bluntness ratio of 0.08 over a range of Reynolds numbers as shown in figure 10. At $\alpha = 50°$, a large side force coefficient was present at the $Re_D = 3.8 \times 10^6$ where a fully turbulent boundary layer separation would be expected, as opposed to the transitional case at $Re_D = 0.8 \times 10^6$ where the side force was very small. However, the maximum side force coefficient at $Re_D = 3.8 \times 10^6$ is about one-half of that for the sharply pointed tangent-ogive in the same reference, suggesting that bluntness also helps at high Reynolds numbers. Blunting the forebody reduces the yawing moment asymmetry, but more data is needed to determine the correct ratio of nose radius to body diameter for fully turbulent flow.

Some wind tunnel tests have shown that nosebooms tend to reduce the yawing moment asymmetry. In figure 11, the yawing moment for an F-15 model with an extended nose was reduced approximately 50 percent at $\alpha = 50°$, and caused an adverse effect on C_{n_β} (fig. 12). This test was conducted in the laminar Reynolds number range, however. Chapman[9] suggested a reduction in yawing moment, but showed no data or other information pertinent to this suggestion. Other wind tunnel data contradict this generalization. Skow[11] cites data from Carr[12] that shows an increase in yawing moment at $\alpha \geq 45°$ for the F-15 with the production nose

and noseboom as compared with the same configuration without a noseboom (fig. 13). This yawing moment asymmetry for the F-15 with a noseboom was confirmed in flight (fig. 14) by the unexpected departure while testing an F-15 with conformal tanks.[13] The same aircraft with conformal tanks, but without the noseboom, showed little yawing moment asymmetry. Skow also shows wind tunnel data for the F-5F (fig. 15) in which the yawing asymmetries became oscillatory with the noseboom rather than biased in one direction.[11] The oscillatory nature of the yawing moment suggested a switching in the forebody vortex system orientation induced by the noseboom wake.

F-18 High Alpha Research Vehicle Flight and Ground Test Results

Extensive wind tunnel and flight experiments were conducted using 0.06- and 0.16-scale F/A-18 wind-tunnel models and the F-18 HARV.[14, 15, 16] The F-18 HARV and both models were extensively instrumented with five rows of pressure orifices on the forebody (fig. 16).

Figure 17 shows a comparison of the forebody pressure distributions from the 0.06 wind-tunnel model and from the F-18 HARV in-flight at $\alpha \approx 40°$.[15] For the data in figure 17(a), the 0.06 model was tested in the Langley Low-Turbulence Pressure Tunnel (LTPT) with and without twin longitudinal no. 180 grit strips located $\pm 54°$ up from the windward plane. With the exception of overpredicting the vortex strength at F.S. 107 (the suction peaks at azmuthal locations of 156° and 204°), the gritting greatly improved correlation of pressure distributions between wind tunnel and flight test experiments. This improvement is apparent at F.S. 142 where the wind tunnel vortex suction peaks and the pressure gradients on the leeward side of the maximum attached flow suction peaks better match the flight measurements. Agreement is also enhanced at F.S. 184.

A similar comparison is made for data from the 0.06 model in the Langley 7- by 10-ft High Speed Tunnel (HST) (fig. 17(b)). Again, the agreement between the flight and the twin grit-strip model is good. In this application, the grit did not produce excessive vortex suction footprints at F.S. 107. In both of these cases, the boundary layer on the wind tunnel models with no grit strips was transitional.

In figure 18, wind tunnel data from the 0.16 model with and without no. 36 twin grit strips at $\pm 54°$ are compared with the flight data at $\alpha \approx 40°$ and $\beta \approx 0°$.[16] As shown in the figure for F.S. 85, the ungritted model data (denoted by the squares), have a *kink* in their pressure distribution near $\theta = 135°$ and 225°. This kink appears to be the result of a laminar separation bubble. The gritted model data, denoted by the circles, do not have a similar kink because the grit strips successfully transitioned the boundary layer to a turbulent state before the boundary layer had an opportunity to separate in a laminar state. At F.S. 85 and F.S. 107, the forebody vortices are more pronounced than for flight, as was seen for the 0.06 model at F.S. 107 above. At F.S. 142, the gritted data agree extremely well with the flight high Reynolds number data for the entire leeward region and, in particular, for the vortex footprints. The gritted data at F.S. 184 also significantly improve the simulation of the flight pressure distributions.

For a case with sideslip, as shown in figure 19, the comparison between the flight data and the model with the twin grit strips is much better than between the flight data and the model with no grit.[16] Smoother recovery pressure gradients occur for the gritted data at all stations. While the gritted data have vortex peaks at F.S. 107 that are moderately too strong, the gritted data more closely match the vortex suction peaks at F.S. 142, particularly at $\theta = 210°$. At F.S. 184, the leeward pressure gradients obtained in flight are much more closely simulated with the gritted data.

The effect of the noseboom on the forebody flow for the 0.06 scale F/A-18 model was shown qualitatively by laser vapor screen image of the forebody at M = 0.6 and $\alpha = 50°$ in figure 20.[17] Figure 20 shows the forebody without the noseboom as having a well-defined vortex pair located on the forebody just forward of the canopy. With the noseboom attached and at the same test conditions, the forebody vortices have been significantly reduced in size, no longer appear as two distinct vortices, and a significant wake emanating from the boom can clearly be seen. An oscillatory motion was also noted in the wind tunnel for the F/A-18 with a noseboom at M = 0.6. Figure 21 shows the variation of the rolling moment and yawing moment coefficients with angle of attack at $\beta = 0°$. The noseboom promoted asymmetric rolling- and yawing-moment coefficients that repeatedly changed sign as the angle of attack increased.

Furthermore, in wind tunnel tests with the 0.16 scale F-18 model, the reduction in directional stability and the reversal in lateral stability is shown with the addition of the noseboom and the forebody flow transitioned by

no. 36 grit strips located on each side at 54° up from the windward attachment line (fig. 22).[18] For the F-18 configuration during wind tunnel tests, gritting the forebody strengthened the forebody vortices by transitioning the forebody to a fully turbulent state from its transitional state. The noseboom attenuated the forebody vortices of the turbulent forebody, reducing the effect of the grit, thereby changing the apparent Reynolds number effects.

The effects of pressure ports on a forebody can be similar to that of grit. If the pressure ports are large enough and dense enough (depending on the model scale) they can cause the flow to transition. Figure 23 shows the lateral-directional results of a 16 percent F-18 model with and without a pressure-instrumented nose at $\alpha = 40°$.[18] The results show a degradation in lateral stability and a shift in C_{l_0}. There are less significant changes in yawing moment, but this trend is similar to the application of grit.

From the previous discussion one should not necessarily assume that the flight vehicle has all turbulent flow on the forebody. Significant laminar flow can exist on smooth forebodies especially at high angles of attack. Figure 24 shows an in-flight surface flow visualization at $\alpha = 47°$, using propylene glycol monomethyl ether and a toluene-based red dye emitted from the pressure orifices.[19] The effect of boundary-layer transition can be noted by the large dye puddle extending intermittently from $\theta = 240°$ at F.S. 70 to almost F. S. 107 at $\theta = 247°$. The puddles are the result of a laminar separation bubble. Note that where the screwhead protuberances around the plugged smoker port (that would cause premature transition) are present, the puddles do not occur. Also notice that the fluid which is windward of the laminar separation bubble, flowed toward the bubble and the fluid that is leeward of the bubble, flowed away. This indicates that the flow reattached turbulently past the very localized laminar separation bubble and that this is not the primary vortex separation line. The laminar flow on the forebody explains why the gritted models, with the grit extended forward of F.S. 107, resulted in excessive vortex peaks, (fig. 17(a) and 18).

Even when laminar boundary layer separation occurs on a forebody, the separation can be asymmetric, resulting in an undesirable yawing moment.[5, 8] Furthermore, if one side has a laminar boundary layer separation and the other side has a turbulent boundary layer separation, then asymmetric side forces can also

occur on the forebody. Pressure distributions from the F-18 HARV for $\alpha = 70°$ are shown in figure 25.[20] Figure 25(a) shows the circumferential pressure distribution on the forebody in the clean configuration. Note the progression of the vortex suction peaks from F.S. 70 to F.S. 142. At F.S. 70, only the port vortex suction peak is apparent. At F.S. 85, the port and starboard vortex peaks are close to the same magnitude. At F.S. 107, the magnitude of the starboard vortex peak is greater than the port vortex peak and at F.S. 142 there is only the starboard vortex peak. At this flight condition, the port side probably has transitional or turbulent boundary layer separation and vortical flow further forward on the nose, resulting in the vortex suction peak on the port side at F.S. 70 and none on the starboard side. Moving aft on the forebody, boundary separation and vortical flow now occurs on the starboard side and results in the suction peak at F.S. 85. At the same time, the port vortex has continued to grow in magnitude and has begun to lift from the surface. Since the port vortex is further from the surface and has less influence on the surface pressures, the port and starboard vortex peaks have about the same magnitude. At F.S. 107 both vortices continue to grow in strength, but the port vortex continues to lift from the surface, resulting in the smaller vortex suction peak on the port side. This process continues on at F.S. 142 where the port vortex has lifted from the surface so that no port vortex suction peak is observed. The starboard vortex has stayed close to the surface and results in a large suction peak at F.S. 142. The proximity of the starboard vortex to the surface has caused the flow to accelerate about the starboard side at F.S. 142 resulting in a higher suction peak at $\theta \approx 70°$ as compared to the suction peak at $\theta \approx 290°$ on the port side. Similar asymmetric pressure distributions can be seen at F.S. 107 and F.S. 184, though to a lesser extent. These asymmetries in the pressure distributions result in a yawing moment to the starboard because of the greater suction pressures on the starboard side.

Figure 25(b) shows the forebody pressure distributions that occur when twin grit strips are applied to the forebody surface 80° from the windward plane on the F-18 HARV. The pressure distributions are much more symmetric with the twin grit strips, especially at F.S. 142, than for the clean configuration shown in figure 24(a).

The effect of only a single grit strip on the port side of the forebody can be seen in figure 25.[20] Figure 25(a) shows the pressure distributions at $\alpha = 67.1°$ which appear similar to the clean configuration at $\alpha = 70°$ (fig. 25(a)) with high suction pressures on the starboard

side. At $\alpha = 69.5°$ (fig. 25(b)) however, the asymmetry has rapidly switched, so that the higher suction pressures are on the port side. This figure shows the effect of different boundary layer conditions on the side of the forebody and how a small change in angle of attack can cause a large shift in asymmetry.

The forebody pressure distributions were integrated for the clean configuration and with grit strips applied to determine the forebody yawing moment, as shown in figure 27.[20] The asymmetries did not become significant until $\alpha = 60°$ for the clean configuration. The twin grit strips reduced the forebody yawing moments to one-fourth of that for the clean configuration. With the single grit strip, the asymmetries became significant starting at $\alpha = 48°$. The single grit strip also caused the forebody yawing moment to switch signs with only a small change in angle of attack.

Qualitative flow visualization data obtained in water tunnels has been shown to be in consistent agreement with smoke flow visualization obtained in low-speed wind tunnels[21] and in flight,[22] in particular for flow emanating from sharp edges, even though the data are at vastly different Reynolds numbers. In figure 28, the leading edge extension (LEX) vortex breakdown location for the F-18 from the water tunnel at very low Reynolds numbers are consistent with data from several wind tunnels at moderate Reynolds numbers and with flight results at high Reynolds numbers. Figure 29 shows the location where the forebody vortex interacts with the LEX vortex for a range of angle of attack. Again, the low Reynolds number data obtained in the water tunnel show excellent agreement with the high Reynolds number flight data.

However, recent data obtained on the F-18 HARV with the actuated forebody strakes[23] show that caution must be exercised in using water tunnel data. Figure 30 shows a comparison of the vortex path of the strake vortex at $\alpha = 30°$. As can be seen in the photos, the strake vortex path for flight and for the David Taylor 8-Ft Wind Tunnel (fig. 30(a) and (b)),[24] travels straight back and is far above the F-18 vertical tails. For the water tunnel case (fig. 30(c)), the strake vortex is apparently drawn down by the LEX vortices flowfield and the strake vortex path is between the vertical tails.

X-29A Forward-Swept Wing Airplane Results

The X-29A airplane is a single place research airplane which integrated several technologies such as the forward-swept wing, aeroelastically-tailored composite

wing and a close-coupled, variable-incidence canard. A 75-inch-long, 3.5 in. maximum-diameter noseboom and a 24-inch-long strake were installed at the nose apex of the X-29 aircraft. The strake was 1.5 in. wide at the apex and 2.5 in. wide at the end. The forebody was extensively instrumented with four circumferential rows of pressure orifices, as shown in figure 31. Pressure measurements were obtained in flight for angles of attack from 15° to 66°.[25] Corresponding pressures were measured at one station, $x/l = 0.136$, on a 1/16 scale model of the X-29 in the National Transonic Facility (NTF) at Reynolds numbers based on wing chord from 0.7×10^6 to 6.8×10^6, M = 0.22 to 0.25 and $\alpha = 30°$ to 66°.

A comparison of X-29A forebody pressure distributions from flight and wind tunnel at corresponding Mach and Reynolds numbers at $x/l = 0.136$ is shown in figure 32. The suction peaks at $\theta \approx 70°$ and 290° in the pressure distribution are caused by the local acceleration of flow around the highly-curved surface at these circumferential angles. The suction peaks at $\theta \approx 150°$ and 210° are a result of the strake and forebody vortices. The comparison of pressure distributions at angles of attack from 30° to 50° show excellent agreement (fig. 32(a)–(c)). However, at angles of attack of 55° and above, the flight data show a distinct asymmetry in the strake-forebody vortex suction footprint. At $\alpha \approx 55°$, (fig. 32(d)), the port strake-forebody vortex causes a large asymmetric suction peak at $\theta \approx 200°$. The starboard strake-forebody vortex from flight lifts from the surface, while the port vortex from flight stays close to the surface and moves inboard. The proximity of the port vortex to the surface and the vortex circulation causes the port-side flow to accelerate more. This results in a larger suction peak at $\theta = 290°$ as compared with $\theta = 70°$ and in a yawing moment to the left.[25] At $\alpha \approx 55°$ the wind tunnel data show a smaller strake-forebody vortex suction peak on the starboard side at $\theta \approx 165°$ as compared with the flight measurements on the port side. However, the suction peaks at $\theta \approx 70°$ and 290° for the wind tunnel show a large asymmetry which would result in a yawing moment to the right. The small vortex suction peak in the wind tunnel suggests that both strake-forebody vortices have lifted, but with the starboard strake-forebody vortex closer to the surface.

At $\alpha \approx 59°$ (fig. 32(e)), a similar asymmetric vortex exists as did at $\alpha \approx 55°$. However, at $\alpha \approx 66°$ (fig. 32(f)), the asymmetry changed signs with the strake-forebody vortex suction peak now on the starboard side at $\theta \approx 160°$, resulting in a yawing moment

to the right. The wind tunnel data did not predict this change in asymmetry.

The possible reasons for the differences at $\alpha = 55°$ and above could be that the X-29A model forebody had a very smooth finish, while the X-29A aircraft forebody had longitudinal gaps and steps caused by the avionics access panels on the forebody, (fig. 33). The model could have had proportionally more laminar flow, resulting in different boundary layer separation characteristics and vortical flow fields.

Additional wind tunnel tests were conducted in the NTF on the X-29 at $\alpha = 66°$. In these tests the Reynolds number was varied from $Re_c = 0.68 \times 10^6$ to 5.1×10^6. The results are shown in figure 34. The Reynolds numbers based on Lamont's criteria from figure 5 range from that of marginally transitional boundary layer separation to that of fully turbulent boundary layer separation. The pressure distributions for the range of transitional separation and turbulent separation have a fair agreement to each other but did not correlate well with the flight data as shown previously in figure 32(f). The highest Reynolds number data in figure 34 did show slight vortex suction peaks. The data at a Reynolds number which would suggest marginally transitional boundary layer separation, $Re_D = 0.31 \times 10^6$, was in poor agreement with, and showed characteristics typical of, a laminar separation. It did not show the suction peaks at $\theta \approx 70°$ and $290°$ but did show slight vortex suction peaks at $\theta \approx 140°$ and $220°$.

Figure 35 shows X-29 wind tunnel pressure distributions with twin grit strips correlated with flight data at $\alpha = 66°$. The no. 80 Carborundum grit strips were applied starting at the nose strake and extending to $x/l \approx 0.23$ and approximately $\pm 80°$ from the windward plane. Grit strip no. 1 was a constant 1/4 in. wide while grit strip no. 2 varied from 1/4 in. wide at the nose strake to 1 in. wide at $x/l \approx 0.23$. Data were obtained with the grit strips at only the lowest Reynolds number, $Re_c = 0.68 \times 10^6$. The correlation of the wind tunnel data to flight at this Reynolds number is improved. Suction peaks at $\theta \approx 70°$ and $290°$ which were absent for tests without grit strips at this Reynolds number (fig. 34) now show better correlation with flight. The flight asymmetry, however, is not present. It would have been interesting to test with grit strips at the highest Reynolds number conditions.

X-31 Enhanced Fighter Maneuverability Demonstrator

Two X-31 research aircraft were built and have been designated ships 1 and 2. The X-31 (fig. 3) featured a single-engine, single-place cockpit and a delta wing. For control each aircraft had a small, forward-mounted canard; single vertical tail with conventional rudder; wing leading flaps; trailing-edge flaps–elevons; and three carbon-carbon paddles for vectoring the jet exhaust.

No surface pressure instrumentation was installed on these aircraft. Each aircraft had a flight test noseboom that protruded from beneath the forebody and extended 125 in. forward to 66.5 in. forward of the nosetip. The diameter of the noseboom was 3.5 in. The flight noseboom configuration, though somewhat unusual, was selected as the best configuration from several that were tested in subscale wind tunnel tests. All the noseboom configurations created adverse changes in the already erratic nature of yawing moment at high angle of attack, but this configuration held the best potential for the flight tests.[26] Large lateral dynamic sting loads were observed with an oscilloscope during these tests of the noseboom configurations; however, large steady-state asymmetric yawing moments were not reported during these wind tunnel tests. The directional divergence parameter, C_{n_β}, dyn, is shown in figure 36 and shows stable values throughout the angle-of-attack range indicating that the configuration should be resistant to yaw departure.[27] Krause,[28] however, showed a maximum C_{n_0} value for the X-31 configuration of 0.05 without a noseboom at low speeds for $\alpha = 60°$ (fig. 37). No data is provided for the model with a noseboom, but nose strakes were shown to be effective in reducing the yawing moments at high angles of attack. The nose strakes were not used in the initial flight testing of the X-31.

During the envelope expansion flights of the X-31 airplane, the pilots reported numerous side-force kicks (which they referred to as "lurches") and other yawing asymmetries above $\alpha = 50°$, especially on ship 2.[29, 30, 20] At this point, the aircraft were carefully weighed and inspected and no geometric asymmetries or differences between the two aircraft were found. Figure 38 shows the yawing moment for the clean forebody configuration for ship 2 as a function of angle of attack for five different 1-g decelerations.[20] As can be seen, the clean forebody produces an asymmetric yawing moment that is very random, although the

magnitude of the asymmetry appears to be bounded at $|C_{n_0}| < 0.080$.

With the success of the boundary-layer transition strips in reducing the forebody yawing moments on the F-18 HARV at high angles of attack,[20] it was decided to try them on the X-31 aircraft (fig. 38). The no. 30 Carborundum grit strips started at the nosetip and ran back approximately 56 in., stopping below the canard leading edge. Since the noseboom was mounted under the forward portion of the forebody, there was a concern over the wake of this noseboom at high angle of attack affecting the forebody vortex development. This concern led to the installation of another transition-strip pair along the noseboom sides at approximately 80° up from the windward plane of symmetry. The goal of using these transition strips was to cause a turbulent separation from the cylindrical boom, thereby minimizing the noseboom wake. Data were obtained with the forebody and noseboom grit strips (fig. 40) in place. The introduction of the forebody and noseboom boundary-layer transition strips results in a more repeatable asymmetry with angle of attack. A band of yawing moment asymmetries which existed for this configuration is shown shaded in figure 40. Although the asymmetry was more predictable with the transition strip than without it, the magnitude of the maximum asymmetry actually increased to almost $|C_{n_0}| = 0.100$. The initial asymmetry was to the right, reaching a maximum of $C_{n_0} = 0.050$ at $48° < \alpha < 54°$. As the angle of attack increased, the asymmetry switched to the left, eventually reaching its maximum asymmetry near $\alpha = 67°$. Although the magnitude of the asymmetry was larger with the transition strip than without it, the pilot comments were generally favorable for the grit strip. This was primarily a result of the reduction in the random behavior of the aircraft with the transition strip in place. With this configuration, the X-31 successfully completed its 1-g flight envelope expansion to $\alpha = 70°$.

In further tests on X-31 ship 2, the transition strips on the noseboom were removed to allow evaluation of the forebody transition strips only. Figure 40 shows the results of the noseboom grit strips from the 1-g flight tests. Two different asymmetry patterns appear as a function of Reynolds number based on noseboom diameter. Data obtained at Reynolds number conditions of $> 3.5 \times 10^5$ have an asymmetry onset at $\alpha = 46°$, a peak asymmetry of $C_{n_0} = -0.070$ at $\alpha = 59°$, and a

small asymmetry again at $\alpha = 70°$. The data obtained at Reynolds numbers $< 2.3 \times 10^5$ during decelerations with forebody grit but without noseboom grit have significantly worse characteristics. The initial asymmetry starts at $\alpha = 38°$ and increases to a level of $C_{n_0} = -0.077$ at $\alpha = 52°$. The asymmetry then rapidly changes signs, increasing to a value of $C_{n_0} = 0.088$ by $\alpha = 55°$. Thus, the total yawing moment change over a 3° angle of attack is 0.165. This was quickly rated as unacceptable by the test pilot. As a result the boundary layer transition strip was reinstalled on the noseboom. These Reynolds numbers based on noseboom diameter coincide very closely with the critical Reynolds numbers for cylinders in crossflow. The lower Reynolds number value is close to the upper bound for laminar flow about a cylinder, 2×10^5, while the higher Reynolds number value is close to the lower bound for turbulent flow, 4×10^5, (fig. 41).[31] The noseboom transition strip caused turbulent boundary layer separation and reduced the sudden changes in yawing moment.

As the elevated-g portion of the envelope expansion began, a departure from controlled flight on the X-31 ship 2 occurred during a 2-g split-S maneuver to $\alpha = 60°$. Data analysis showed that the departure was triggered by a large unmodeled yawing moment. The yawing moment increment was calculated and is shown in figure 42. A peak yawing moment value of 0.125 is shown, although the departure initiates before the peak value is reached. The departure made it clear that the boundary layer transition strips were not sufficient to complete the elevated-g, high-angle-of-attack envelope clearance.

The X-31 project was forced to try more intrusive configuration changes to control the forebody yawing moment asymmetries. A wind-tunnel test of several strake configurations was completed in the NASA Langley Research Center 30-by-60-ft wind tunnel.[32] The large amplitude asymmetry measured in flight was not predicted in the wind-tunnel test; however, some asymmetry was found over the same angle-of-attack range (fig. 43). A 0.6-in.-wide by 20-in.-long (full-scale dimensions) strake reduced the asymmetry on the model. This strake design was manufactured and installed on both X-31 aircraft (fig. 44). The aircraft nose apex was also rounded to more nearly match the wind-tunnel model ($r = 0.75$ in., $2r/D = 0.039$ on ship 1 and $r = 0.5$ in., $2r/D = 0.026$ on ship 2). While the noseboom complicates the flow somewhat, the initial X-31 nose radius ($2r/D = 0.003$), as shown in figure 45, would be expected to be prone to forebody asymmetries and might

be improved with further blunting. Also shown in figure 45 are the nose radius ratios for the F-18 HARV and F/A-18 aircraft. Both of these configurations have acceptable nose radii, if the merits of reference 11 are applied. Flight tests of the X-31 aircraft confirmed that the strake and noseboom grit strip modifications did reduce the asymmetry to a level that could be compensated for by the control system; however, a significant amount remained (fig. 46). Figure 46 also shows the beneficial effect of grit on the noseboom. The grit on the noseboom, combined with the nose strakes, reduced the yawing moment asymmetry and eliminated the yawing moment reversal.

The X-31 wind tunnel tests that were performed before the flight tests gave very little indication of the large asymmetric yawing moments that would be encountered in flight. During wind tunnel tests to determine the best strake configuration, in the Langley 30-by-60 ft. wind tunnel, data were also obtained for the X-31 model with just one strake to assess the level of asymmetry that could be generated.[29] Those results are compared with the X-31, ship 2, asymmetry characteristics for the clean configuration (fig. 47). As can be seen, the wind tunnel data from the single-strake configuration was a good indicator of the maximum yawing moment that was encountered in flight for the clean configuration.

The X-31 reaffirmed the requirement to test the same configurations in flight and in the wind tunnel. The flight yawing moments at flight Reynolds numbers were larger than those measured in the wind tunnel for the same configuration at low Reynolds numbers. Reynolds numbers effects on seemingly unimportant items, such as the noseboom, were also shown to cause serious flying qualities problems.

Concluding Remarks

Lessons learned from ground based tests to flight correlations for the high-angle-of-attack programs on the F-18 High Alpha Research Vehicle (HARV), the X-29 forward-swept wing aircraft and the X-31 enhanced fighter maneuverability aircraft have been presented. On all three vehicles Reynolds number effects were evident on the forebodies at high angles of attack. Pressure distributions on the forebody were compared from flight to wind tunnel for both the F-18 HARV and the X-29. The correlation between flight and wind tunnel pressure distributions for the F-18 HARV were improved by using twin longitudinal grit strips on the forebody of the wind-tunnel model. Pressure distributions obtained on the X-29 wind-tunnel model at

flight Reynolds numbers showed excellent correlation with the flight data up to $\alpha = 50°$. Above $\alpha = 50°$, the pressure distributions for both flight and wind tunnel became asymmetric and showed poorer agreement, possibly because the surface finish of the model was different than the aircraft. The effect of a very sharp nose apex was demonstrated on the X-31. The X-31 showed that nose strakes can reduce forebody asymmetries. The grit on the noseboom, combined with the nose strakes, reduced the yawing moment asymmetry and eliminated a yawing moment reversal. Grit strips on the forebody of the X-31, however, increased the magnitude of the asymmetry but reduced the randomness of the asymmetry.

Recommendations

The following recommendations for wind tunnel and flight testing are suggested to enhance wind-tunnel-to-flight correlation at high angles of attack.

To ensure fewer surprises in flight testing, test wind-tunnel models at high angles of attack with a standard nose grit ring, and with a standard nose grit ring combined with twin symmetric grit strips. To ensure that the flight control system can overcome the largest forebody asymmetries possible, also test the model with a nose strake on one side only.

For obvious reasons, be certain that the wind tunnel and flight vehicle have the same configuration, i.e., nose radius, noseboom position (if included), protuberances, joints and gaps, etc.

To reduce the effect of a flight test noseboom on the lateral-directional characteristics of the aircraft, apply twin grit strips on the aircraft flight test boom to minimize the noseboom wake and its repercussions.

References

[1]Chambers, Joesph R., William P. Gilbert, and Luat T. Nguyen, *High Angle-of-Attack Technology*, vol. 1, part 1–3, NASA CP-3149, May 1992.

[2]Matheny, Neil W., *High-Angle-of-Attack Projects and Technology Conference*, vol. 1–4, NASA CP-3207, Apr. 1992.

[3]Anon: *Fourth High Alpha Conference*, vol. 1–3, NASA CP-10143, July 1994.

[4]Chambers, Joseph R., James R. Burley and Robert R. Meyer, *High-Angle-of-Attack Technology Accomplishments, Lessons Learned, and Future Directions*, NASA/CP-1998-207676/PT1, PT2, and PT 3, June 1998.

(Note: ITAR restricted. Distribution is limited; other requests shall be referred to Patricia A. West, M/S 246A, Langley Research Center, Hampton, Virginia 23681.

[5]Lamont, P. J., "Pressures Around an Inclined Ogive Cylinder with Laminar, Transitional, or Turbulent Separation," AIAA Journal, vol. 20, no. 11, pp. 1492–1499, Nov. 1982.

[6]Hall, Robert M., "Influence of Reynolds Number on Forebody Side Forces for a 3.5 Diameter Tangent-Ogive Bodies," AIAA Paper 87-2274, 1987.

[7]Keener, Earl R., Flow Separation Patterns on Symmetric Forebodies, NASA TM-86016, Jan. 1986.

[8]Hunt, B. L., "Asymmetric Vortex Forces and Wakes on Slender Bodies" (Invited Paper), AIAA-82-1336, Aug. 1982.[#]

[9]Chapman, Gary T., Earl R. Keener, and Gerald N. Malcolm, "Asymmetric Aerodynamic Forces on Aircraft Forebodies at High Angles of Attack—Some Design Guides," AGARD CP-199, paper 12, June 1976.

[10]Keener, Earl R., Gary T. Chapman, Lee Cohen, and Jamshid Taleghani, Side Forces on a Tangent Ogive Forebody with a Fineness Ratio of 3.5 at High Angles of Attack and Mach Numbers from 0.1 to 0.7, NASA TM X-3437, Feb. 1977.

[11]Skow, A. M. and G. E. Erickson, "Modern Fighter Aircraft Design for High-Angle-of-Attack Maneuvering," AGARD LS-121, paper 4, 1982.[**]

[12]Carr, Peter C. and William P. Gilbert, Effects of Fuselage Forebody Geometry on Low-Speed Lateral-Directional Characteristics of Twin-Tail Fighter Model at High Angles of Attack, NASA TP-1592, Dec. 1979.

[13]Bass, Mark D., "Results of High Angle-of-Attack Testing of the F-15 with Conformal Fuel Tanks," Society of Flight Test Engineers 15th Annual Symposium Proceedings, 1984.[††]

[14]Fisher, David F., Daniel W. Banks, and David M. Richwine, F-18 High Alpha Research Vehicle Surface Pressures: Initial In-Flight Results and Correlation With Flow Visualization Results and Wind-Tunnel Data, NASA TM-101724, Aug. 1990.

[15]Hall, R. M., D. W. Banks, D. F. Fisher, F. Ghaffari, D. G. Murri, J. C. Ross, and W. R. Lanser, "A Status Report on High Alpha Technology Program (HATP) Ground Tests to Flight Comparisons," NASA CP-10143, vol. 1, July 1994.

[16]Hall, Robert M., William G. Sewall, Daniel G. Murri, Dennis O. Allison, and Daniel W. Banks, "Simulating High Reynolds Number Flows at High-α with Advanced Forebody Gritting Patterns," presented at High Angle of Attack Conference, NASA Langley Research Center, Hampton, Virginia, Sept. 1996.

[17]Erickson, Gary E., Wind Tunnel Investigation of Vortex Flows on F/A-18 Configuration at Subsonic Through Transonic Speeds, NASA TP-3111, Dec. 1991.

[18]Banks, Daniel W., David F. Fisher, Robert M. Hall, Gary E. Erickson, Daniel G. Murri, Sue B. Grafton, and William Sewall, The F/A-18 High Angle-of-Attack Ground-to-Flight Correlation: Lessons Learned, NASA TM 4783, Jan. 1997.

[19]Fisher, David F., John H. Del Frate, and David M. Richwine, In-Flight Flow Visualization Characteristics of the NASA F-18 High Alpha Research Vehicle at High Angles of Attack, NASA TM-4193, May 1990.

[20]Fisher, David F. and Brent R. Cobleigh, Controlling Forebody Asymmetries in Flight—Experience With Boundary Layer Trips, NASA TM-4595, July 1994.

[21]Erickson, Gary E., Water Tunnel Flow Visualization and Wind Tunnel Data Analysis of the F/A-18, NASA CR-165859, May 1982.

[22]Del Frate, John H. and Fanny A. Zuniga, "In-Flight Flow Field Analysis of the NASA F-18 High Alpha Research Vehicle With Comparison to Ground Facility Data," AIAA-90-0231, Jan. 1990.

[23]Fisher, David F., Daniel G. Murri, and Wendy R. Lanser, Effect of Actuated Forebody Strakes on the Forebody Aerodynamics of the NASA F-18 HARV, NASA TM-4774, Oct. 1996.

[24]Erickson, Gary E. and Daniel G. Murri, Wind Tunnel Investigations of Forebody Strakes for Yaw Control on

[#]Through the courtesy of Mr. B. L. Hunt, Northrop Corporation, Hawthorne, California, and the American Institute of Aeronautics and Astronautics, Washington, D.C.

[**]Through the courtesy of Northrop Grumman Corporation, El Segundo, California. The original version of this material was first published by the Advisory Group for Aerospace Research and Development, North Atlantic Treaty Organization (AGARD/NATO) in Lecture Series LS.121 on High Angle-of-Attack Aerodynamics in December 1982.

[††]Through the courtesy of Mr. Mark D. Bass, McDonnell Aircraft Company, McDonnell Douglas Corporation, St. Louis, Missouri, and of the Society of Flight Test Engineers.

F/A-18 Model at Subsonic and Transonic Speeds, NASA TP-3360, Sept. 1993.

[25]Fisher, David F., David M. Richwine, and Stephen Landers, *Correlation of Forebody Pressures and Aircraft Yawing Moments on the X-29A Aircraft at High Angles of Attack*, NASA TM-4417, November 1992, also published as AIAA-92-4105, Aug. 1992.

[26]Banks, Daniel W., Gregory M. Gatlin, and John W. Paulson, Jr., *Low-Speed Longitudinal and Lateral-Directional Aerodynamic Characteristics of the X-31 Configuration*, NASA TM-4351, Oct. 1992.

[27]Croom, Mark A. and Harvey G. Schellenger, *High-Alpha Flight Dynamics of the X-31 Configuration*, NASA CP-3149, part 3, vol. 1, pp. 1315–1352, 1990, (ITAR).

[28]Krause, Werner, *Aerodynamic Development of the X-31 Aircraft for the High Angle of Attack Region*, MBB-FE211-S-PUB-452, May 1991.

[29]Cobleigh, Brent R., Mark A. Croom, and B. F. Tamrat, "Comparison of X-31 Flight, Wind Tunnel, and Water Tunnel Yawing Moment Asymmetries at High Angles of Attack," NASA CP-10143, vol. 1, July 1994.

[30]Cobleigh, Brent R., *High-Angle-of-Attack Yawing Moment Asymmetry of the X-31 Aircraft from Flight Test*, AIAA 94-1803, June 1994, also published as NASA CR-186030, Sept. 1994.

[31]Shevell, Richard S., *Fundamentals of Flight*, Prentice-Hall Inc., Englewood Cliffs, NJ, 1983.

[32]Croom, Mark A., David J. Fratello, Raymond D. Whipple, Matthew J. O'Rourke, and Todd W. Trilling, "Dynamic Model Testing of the X-31 Configuration for High-Angle-of-Attack Flight Dynamics Research," AIAA 93-3674, 1993.

Figure 1. F-18 High Alpha Research Vehicle.
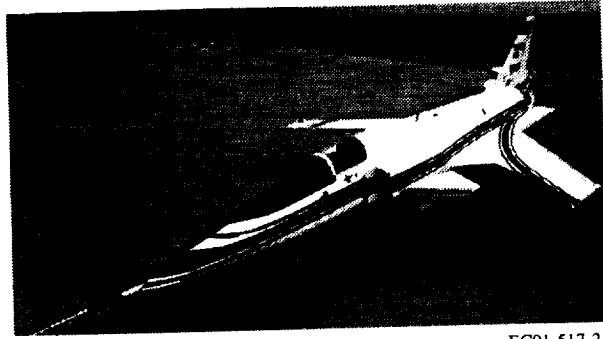
Figure 2. X-29 forward-swept wing aircraft.
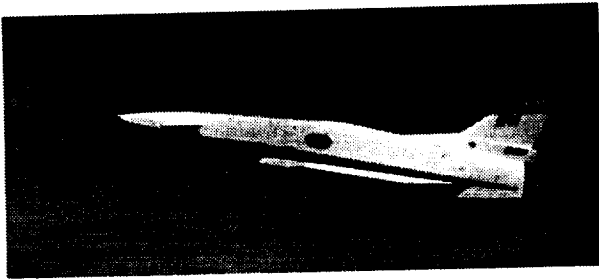
Figure 3. X-31 enhanced fighter maneuverability demonstrator.
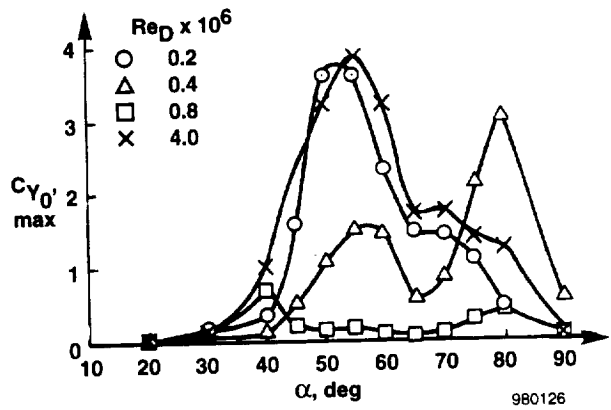
Figure 4. Variation of maximum overall side force coefficient with angle of attack.[5]
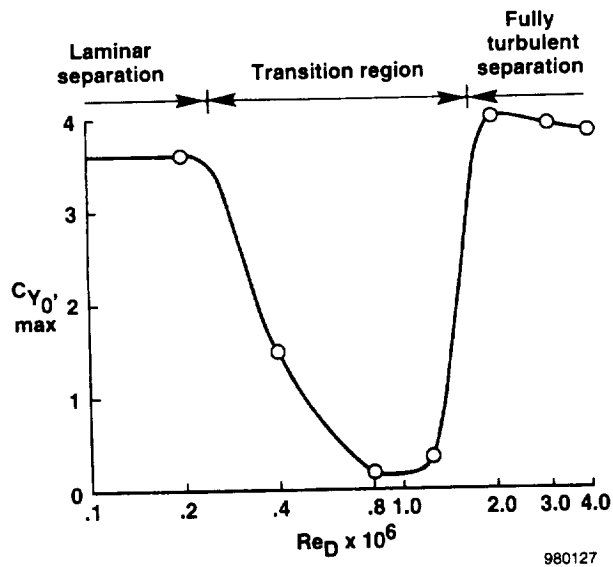
Figure 5. Variation of maximum overall side force coefficient with Reynolds number, $\alpha = 55°$.[5]
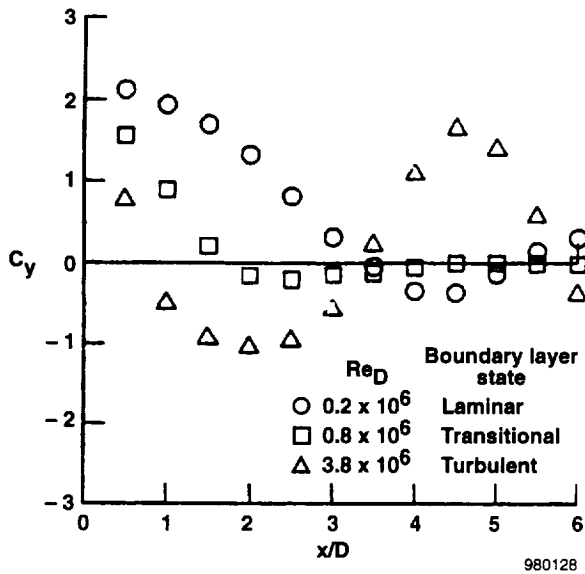
Figure 6. Effect of Reynolds number on sectional side force coefficient.[6]
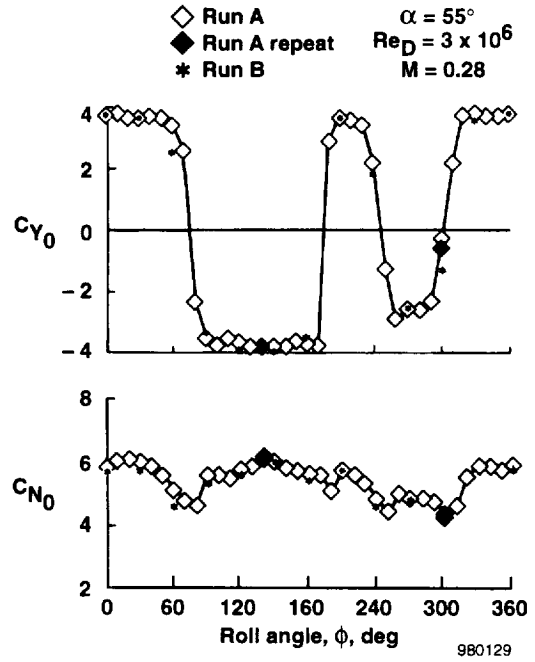
Figure 7. Variation of side force coefficent with roll angle.[5]
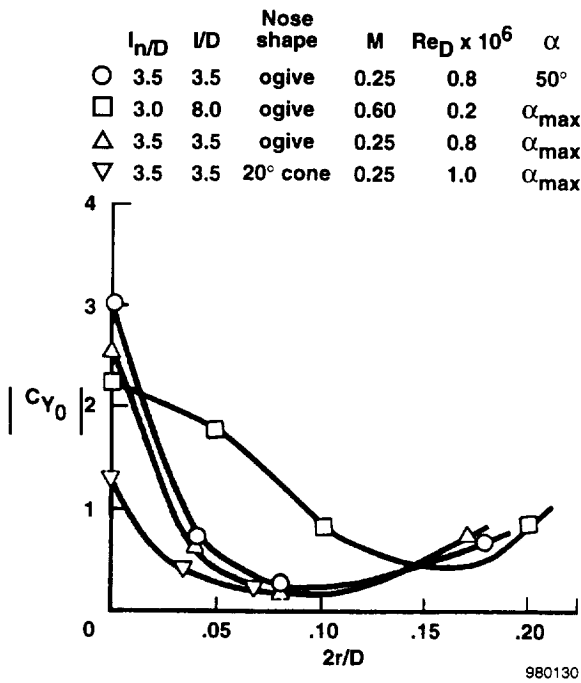
Figure 8. Effect of nose bluntness on side force coefficient for several bodies.[8]
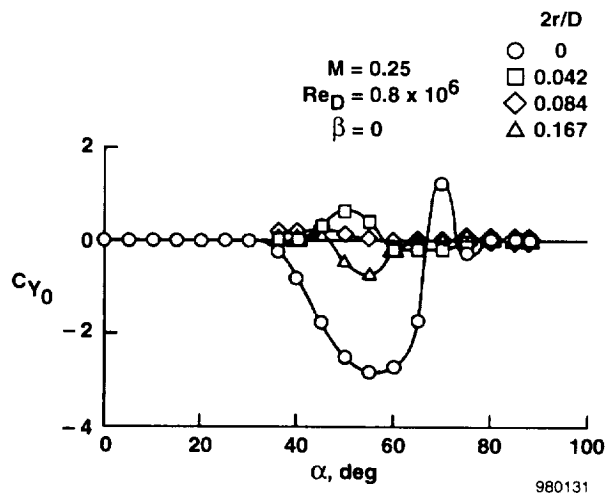
Figure 9. Effect of nose bluntness on side force coefficient for a 3.5 tangent ogive.[9]

13
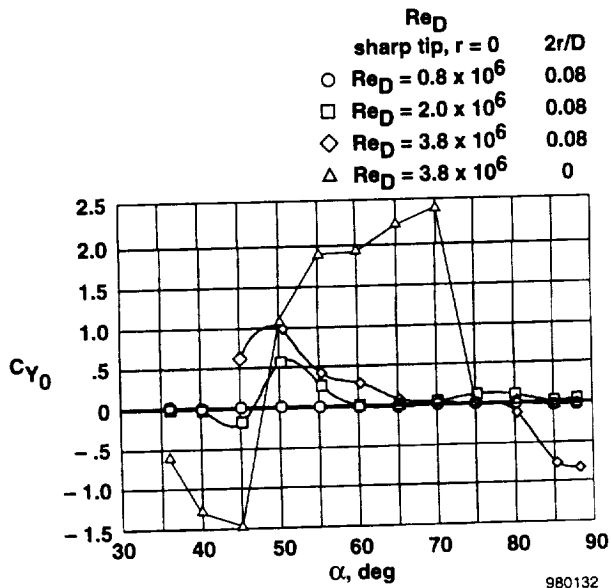
Figure 10. Effect of Reynolds number with nose bluntness on side force coefficient.[10]
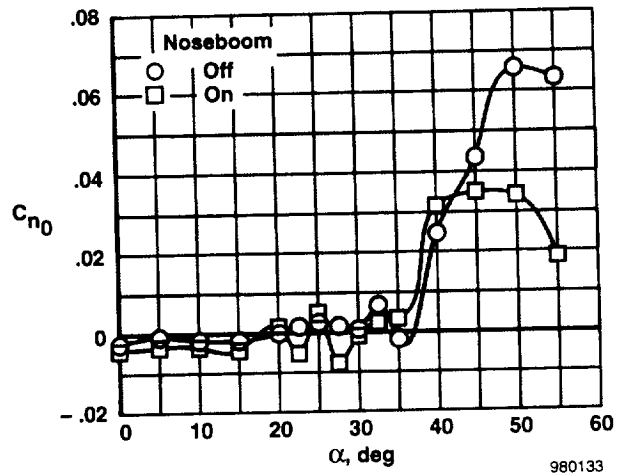
Figure 11. Effect of noseboom on F-15 yawing moment coefficient with extended nose, $\beta = 0°$.[12]
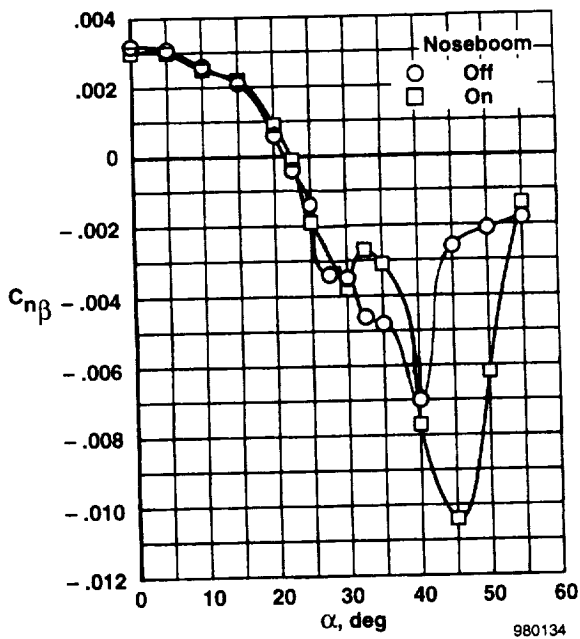
Figure 12. Effect of noseboom on static directional stability parameter.[12]
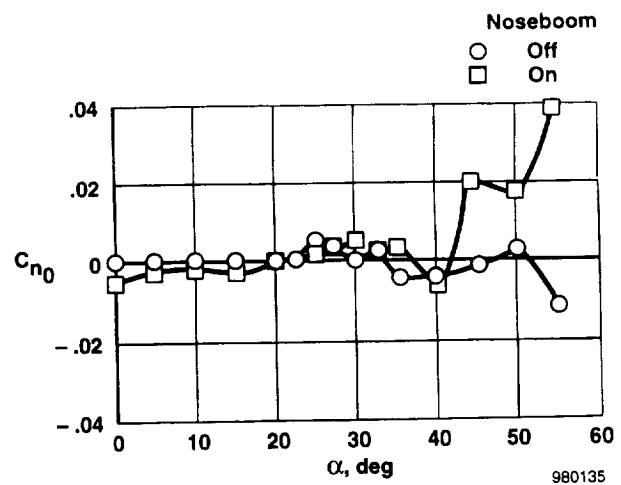
Figure 13. Effect of noseboom on F-15 yawing moment coefficient with production nose, $\beta = 0°$.[11]

14
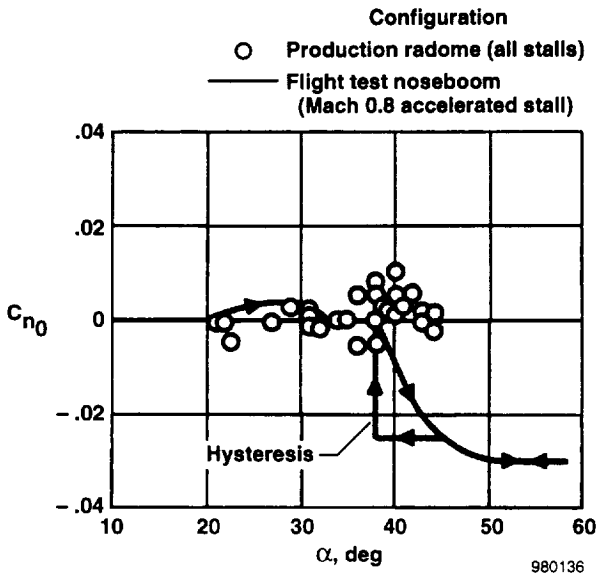
Figure 14. Effect of noseboom on F-15 yawing moment from flight.[13]
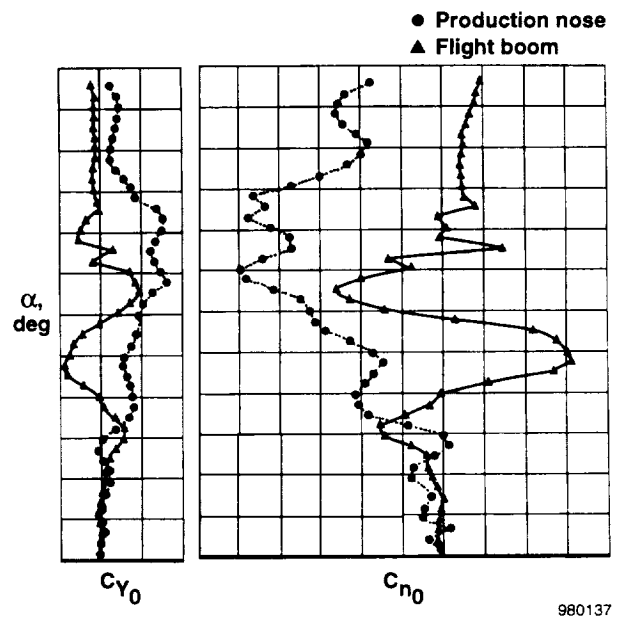
Figure 15. Effect on noseboom on F-5F yawing moment.[11]
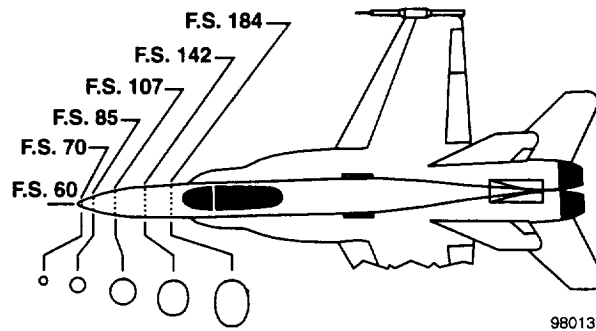
Figure 16. F-18 HARV forebody surface static pressure instrumentation.

Test	Grit	α, deg	β, deg	M_∞	$Re_c \times 10^6$	$Re_D \times 10^6$
—— LTPT	Twin, no. 180	40.0	0.0	0.30	1.41	0.50
- - - LTPT	No grit	40.0	0.0	0.30	1.41	0.50
O Flight	No grit	39.7	−0.3	0.25	9.57	3.41

(a) Correlation with LTPT.

Test	Grit	α, deg	β, deg	M_∞	$Re_c \times 10^6$	$Re_D \times 10^6$
—— 7 x 10	Twin, no. 180	39.4	0.1	0.30	1.39	0.50
- - - 7 x 10	Nose ring only	40.3	0.0	0.30	1.36	0.48
O Flight	No grit	39.7	−0.3	0.25	9.57	3.41
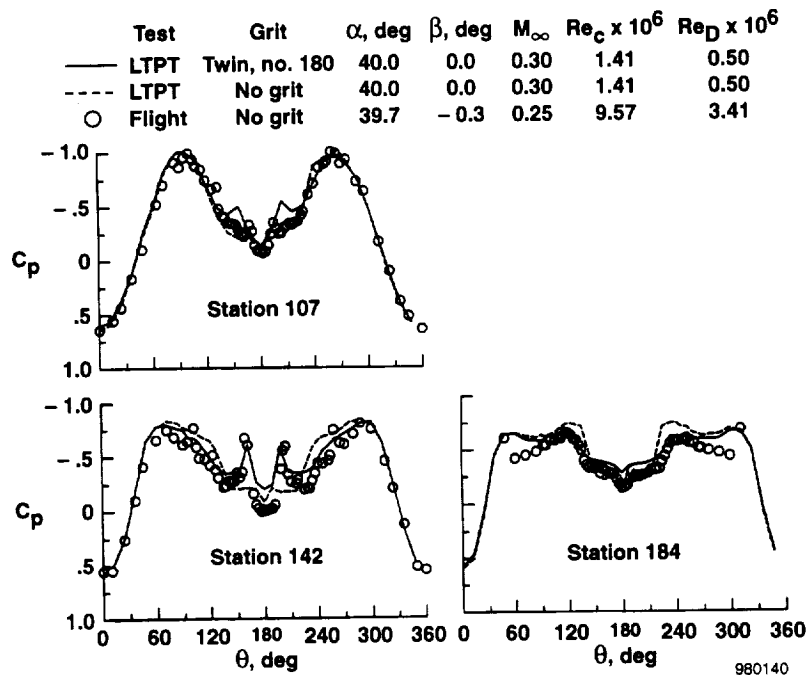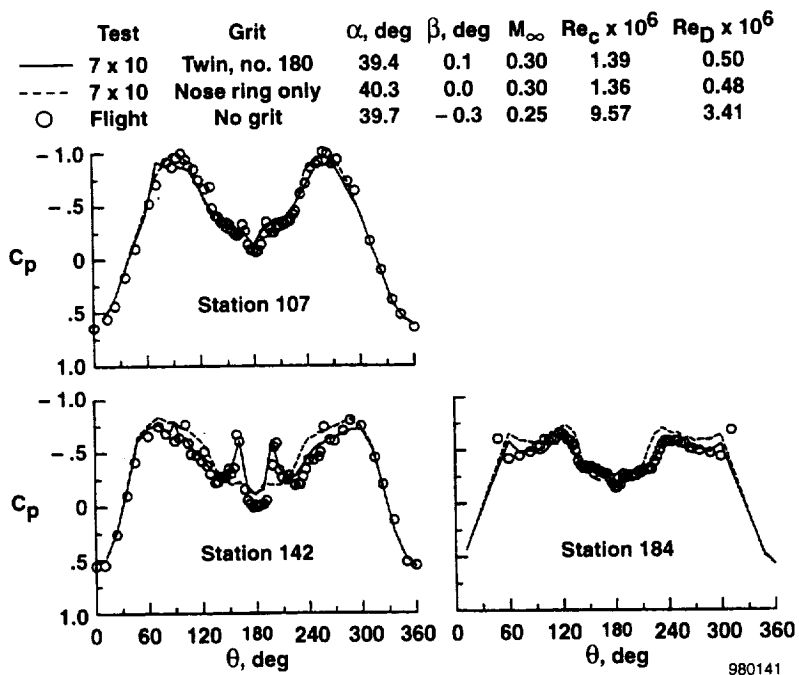
(b) Correlation with 7-by-10-ft HST.

Figure 17. Correlation of 0.06 scale F-18 wind tunnel forebody pressure distributions with and without gritting to flight results.[15]
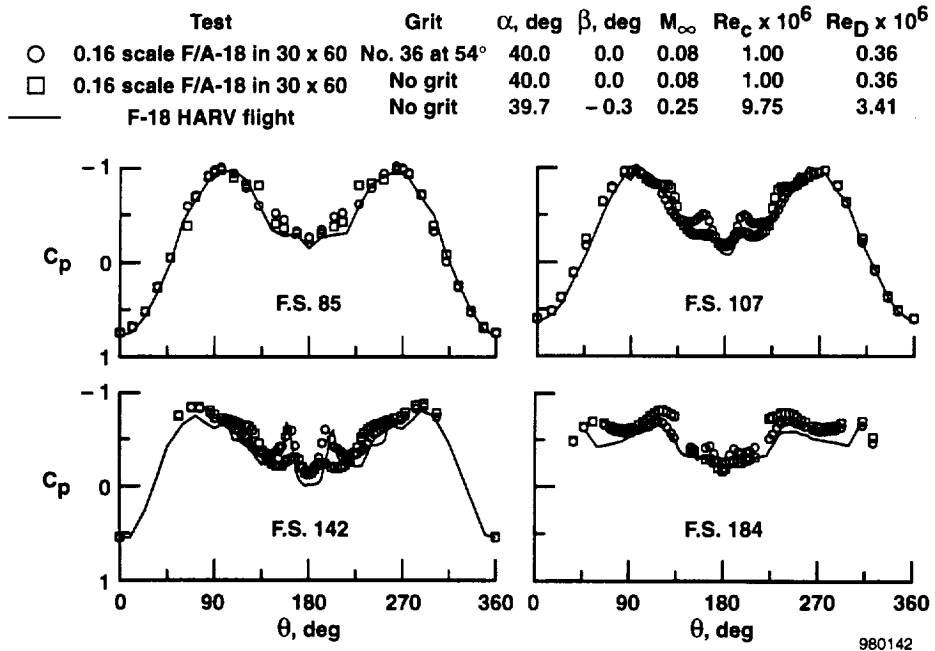
Figure 18. Correlation of 0.16 scale F-18 model data with and without grit strips to flight data, $\alpha = 40°$, $\beta = 0°$.[16]
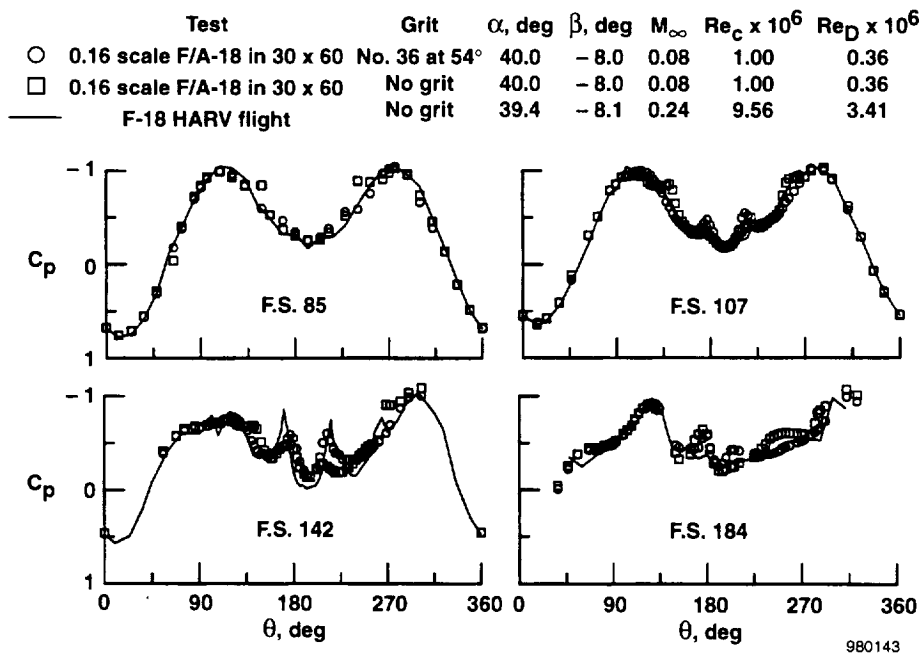
Figure 19. Correlation of 0.16 scale F-18 model data with and without grit strips to flight data, $\alpha = 40°$, $\beta = -8°$.[16]

American Institute of Aeronautics and Astronautics
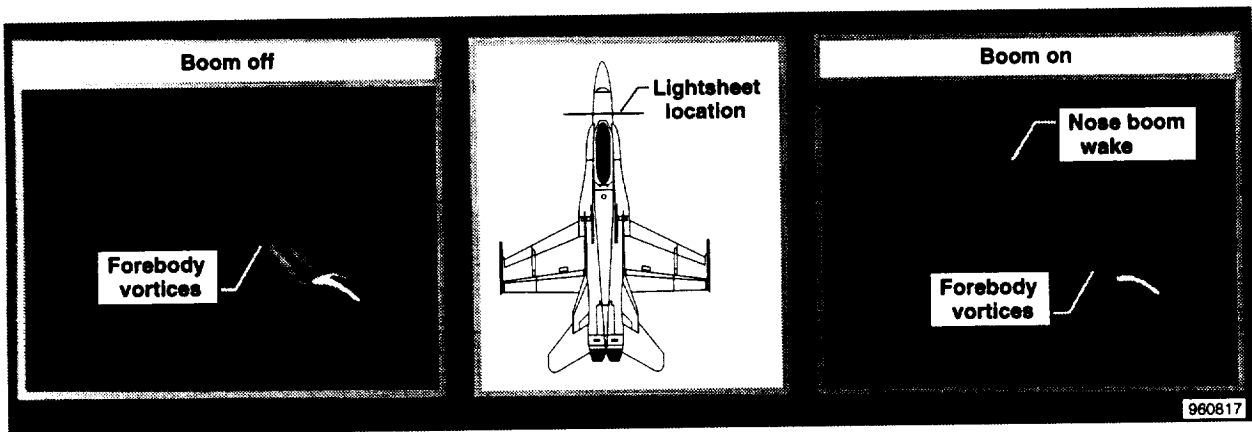
Figure 20. Flow visualization of 0.06 F/A forebody with and without noseboom. $\alpha = 50°$, $\beta = 0°$, M = 0.6, F.S. = 184, $Re_c \approx 1.3 \times 106$, $Re_D \approx 0.4 \times 106$.[17, 18]
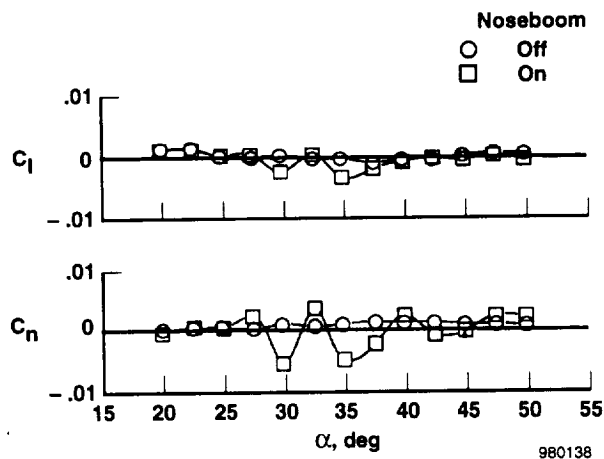
Figure 21. Effect of noseboom on the F-18 lateral-directional characteristics at M = 0.6, Re_c = 1.32 × 10^6 and $\beta = 0°$.[17]

18
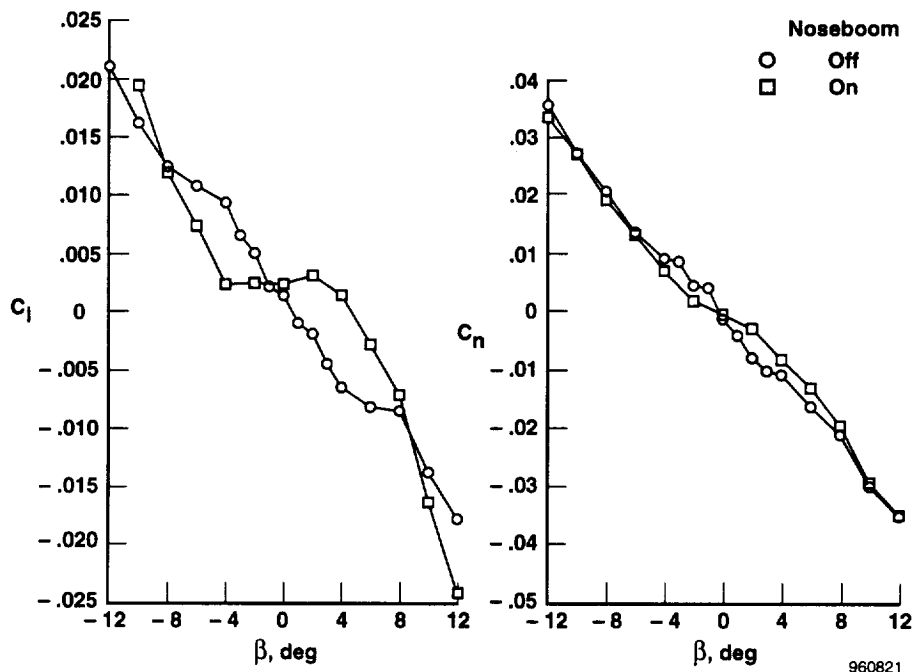
Figure 22. Effect of noseboom on lateral-directional aerodynamics of 0.16 F/A-18 model. $\alpha = 40°$, $\beta = 0°$, M = 0.08, $Re_c \approx 1 \times 10^6$, $Re_D \approx 0.3 \times 10^6$, twin no. 36 grit strips.[18]
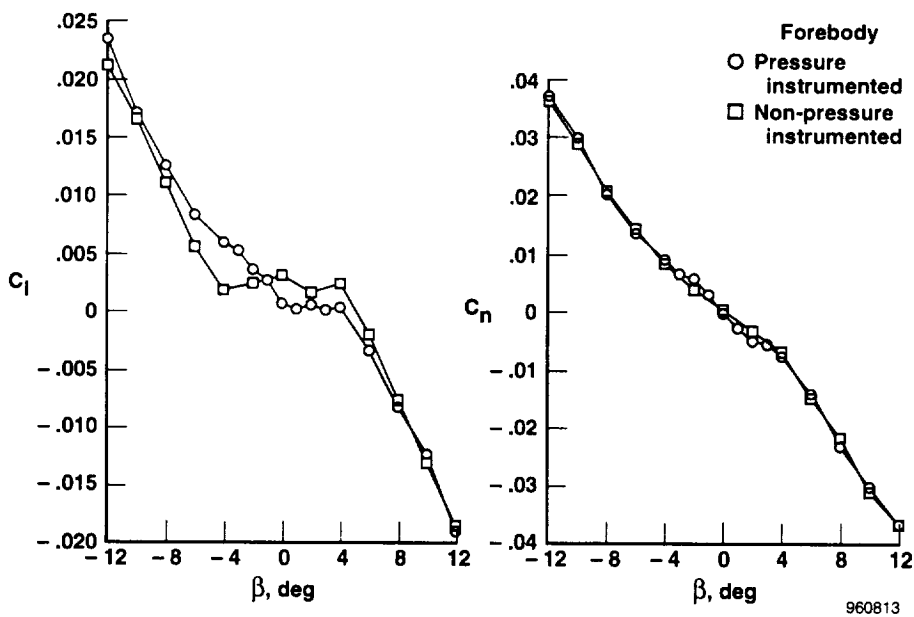
Figure 23. Effect of pressure ports on lateral-directional aerodynamics of 0.16 scale F/A-18 model in the NASA Langley 30-x 60-ft Tunnel. $\alpha = 40°$, M = 0.08, $Re_c \approx 1 \times 10^6$, $Re_D \approx 0.3 \times 10^6$.[18]

19

(b) α = 69.5°, β = -0.7°.

Figure 26.   Concluded.

O Dryden water tunnel, $Re_c = 8.3 \times 10^3$
■ Flight, $Re_c = 8 \times 10^6$ to 13×10^6

α, deg

x/l

● Flight, $Re_c = 8 \times 10^6$ to 13×10^6
▲ DTRC 7 x 10 transonic tunnel, $Re_c = 1.75 \times 10^6$
△ BART wind tunnel, $Re_c = 1.6 \times 10^5$
O McAir LSWT, $Re_c = 3.6 \times 10^5$
□ Dryden water tunnel, $Re_c = 12.6 \times 10^3$

α, deg

x/l

10100
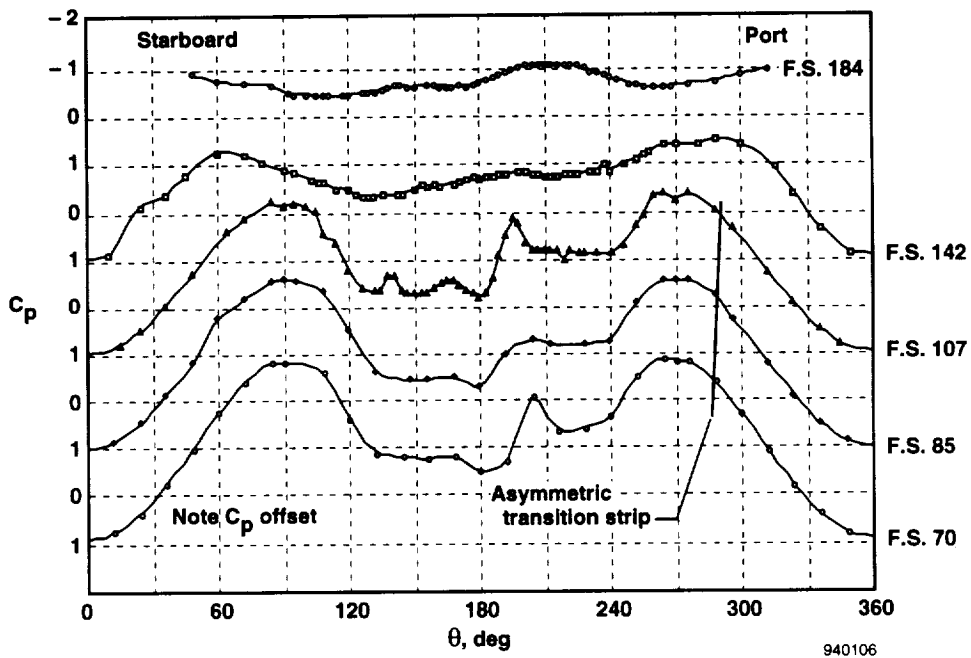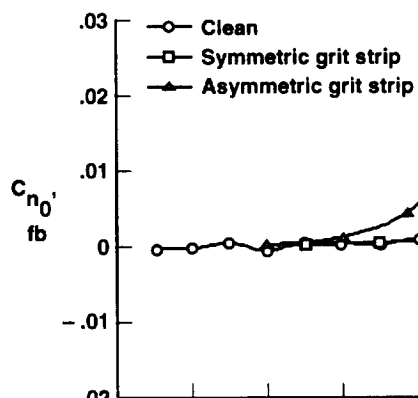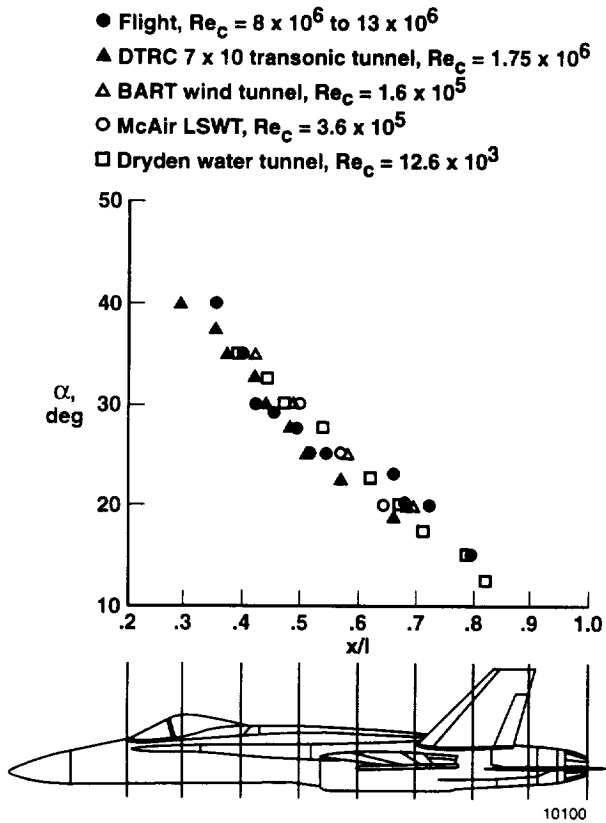
Figure 28. Comparison of F-18 LEX vortex core breakdown between flight and ground facilities.[22]

.3

.4

.5

.6

10126
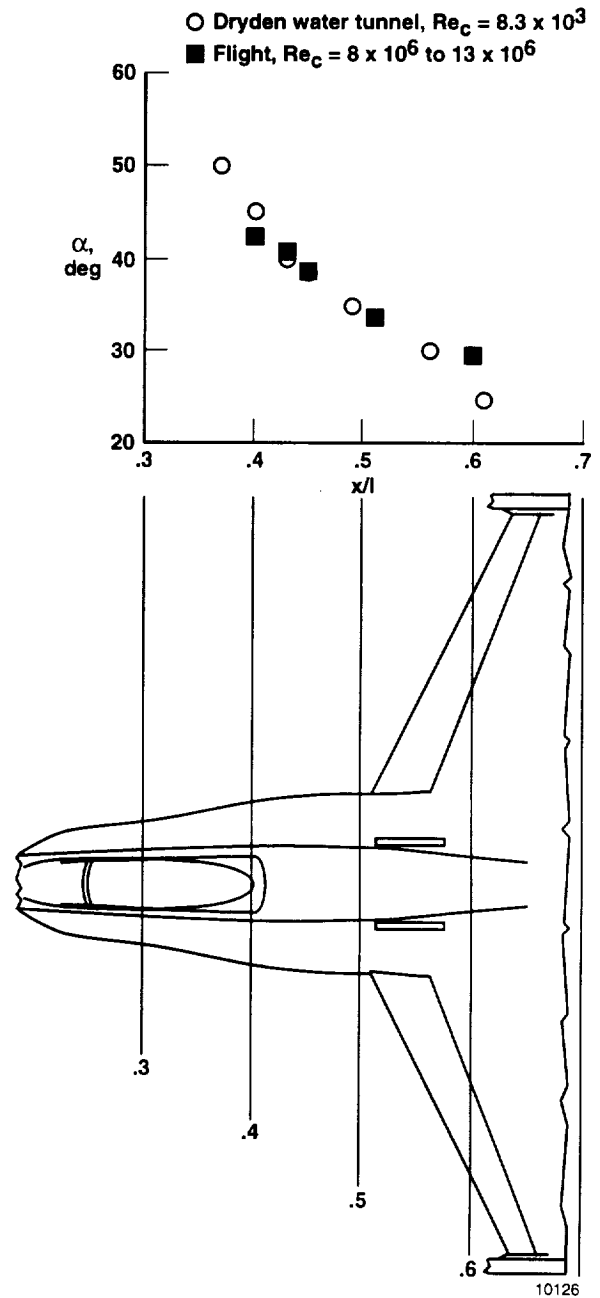
Figure 29. Comparison of F-18 forebody and LEX vortex interaction location from flight and water tunnel.[22]
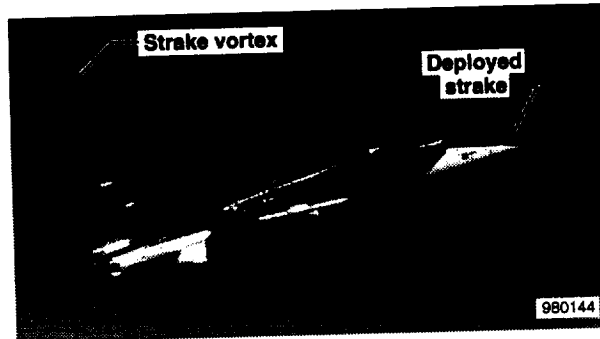
(a) Flight.

(b) Wind tunnel.
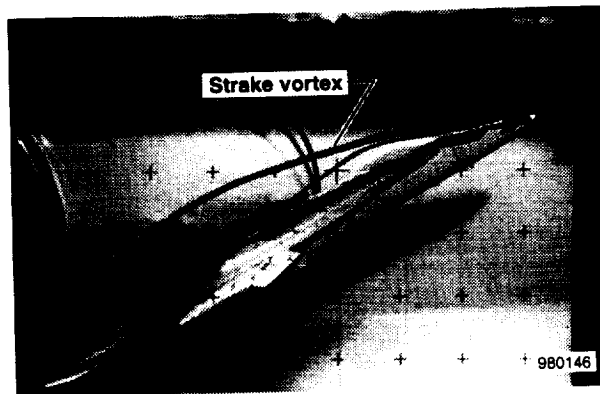
(c) Water tunnel.

Figure 30. Comparison of F-18 forebody strake vortex path from flight, wind tunnel and water tunnel.[24]
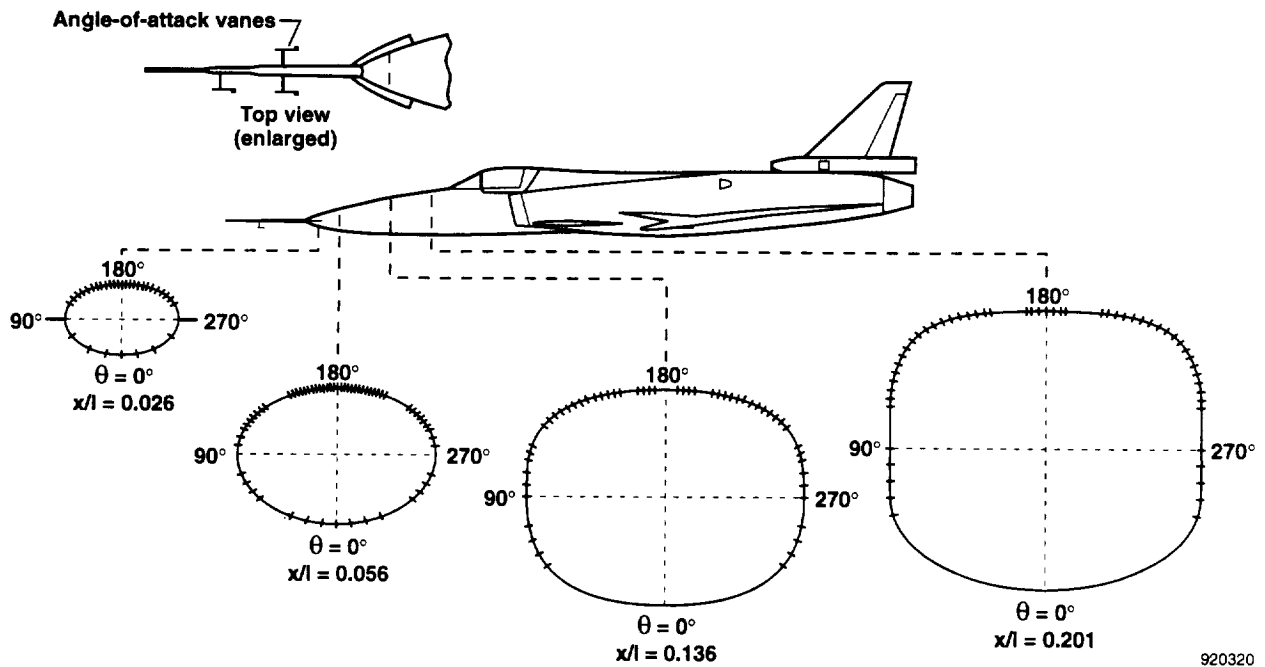
Figure 31. Location of pressure orifices on the X-29A forebody, cross-sectional view from in from of aircraft.[25]

(a) $\alpha \approx 30°$.

(b) $\alpha \approx 40°$.
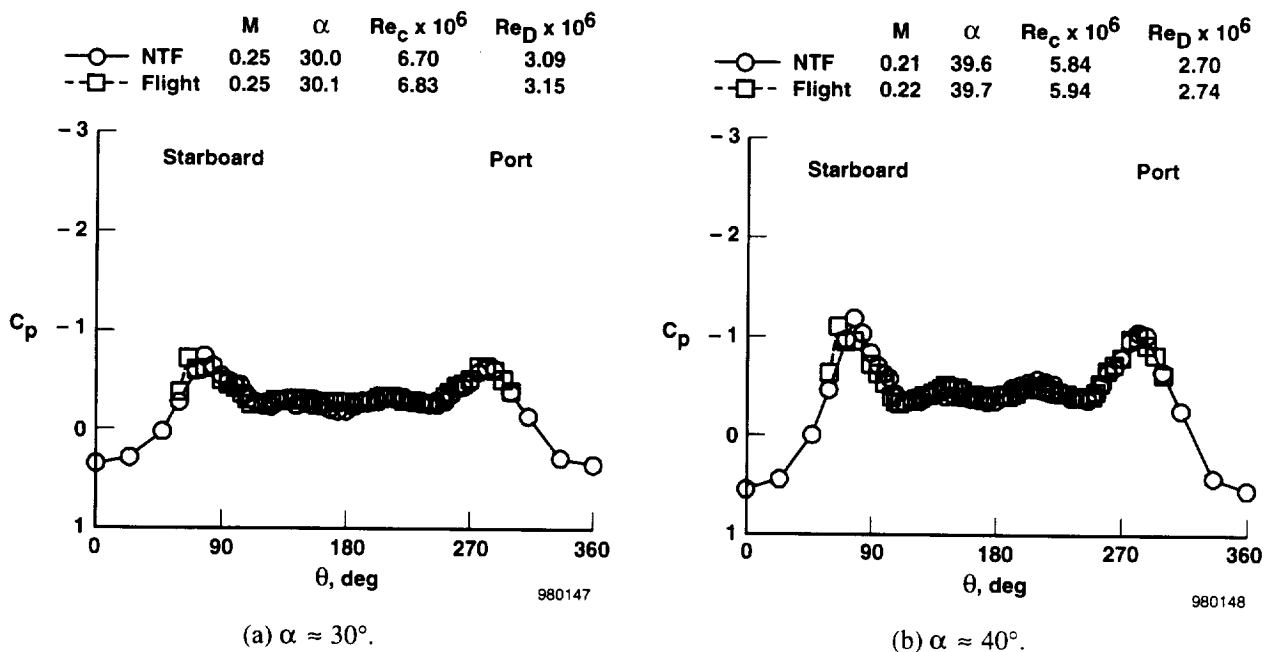
Figure 32. Comparison of X-29A forebody pressure distributions from flight and NTF wind tunnel, $x/l = 0.136$.

	M	α	$Re_c \times 10^6$	$Re_D \times 10^6$
NTF	0.22	49.6	5.53	2.55
Flight	0.23	49.7	5.67	2.62

(c) $\alpha \approx 50°$.

980149

	M	α	$Re_c \times 10^6$	$Re_D \times 10^6$
NTF	0.23	54.6	5.31	2.45
Flight	0.23	54.7	5.41	2.50

(d) $\alpha \approx 55°$.

980150

	M	α	$Re_c \times 10^6$	$Re_D \times 10^6$
NTF	0.23	59.0	5.35	2.47
Flight	0.23	59.1	5.44	2.51

(e) $\alpha \approx 59°$.

980151

	M	α	$Re_c \times 10^6$	$Re_D \times 10^6$
NTF	0.22	66.0	5.11	2.36
Flight	0.22	66.2	5.18	2.39

(f) $\alpha \approx 66°$.
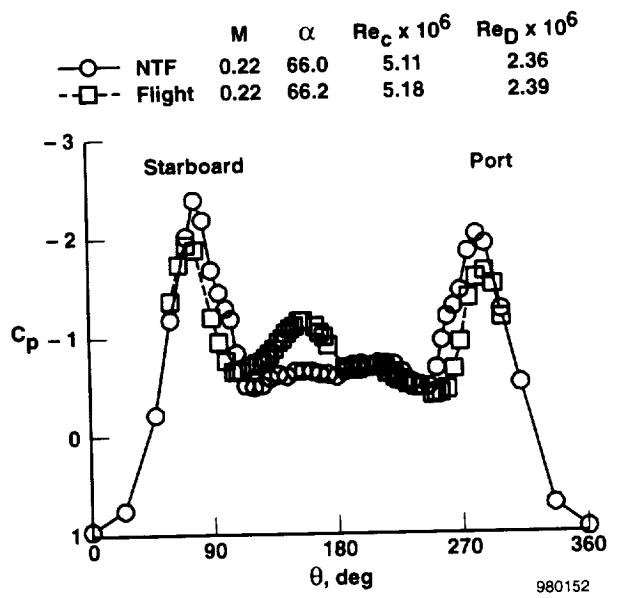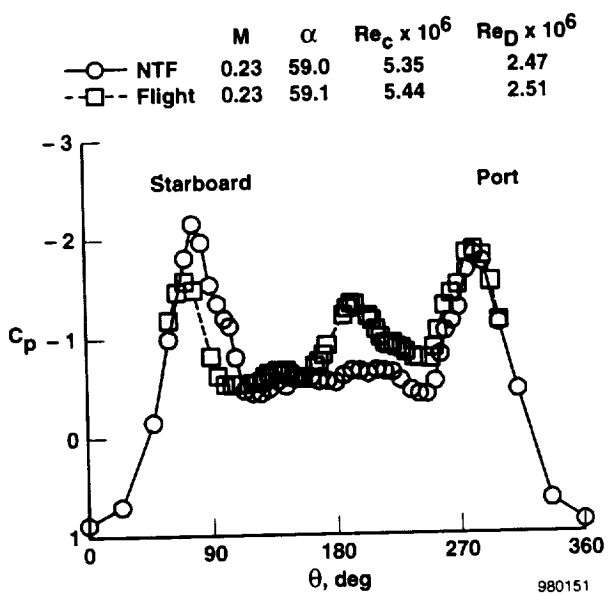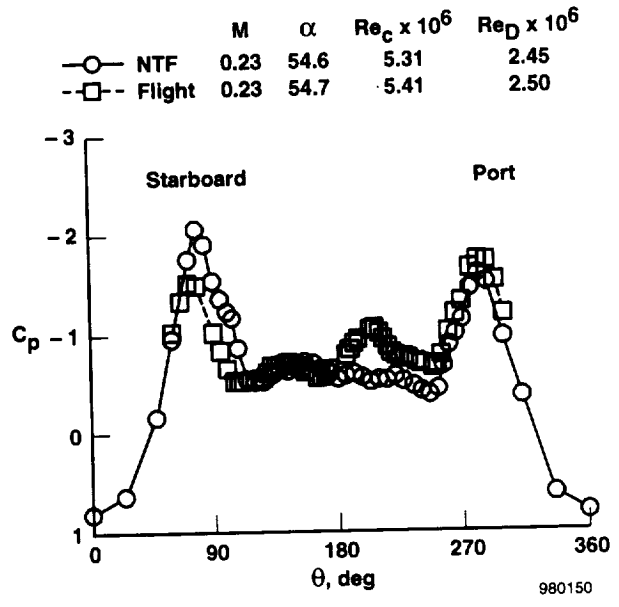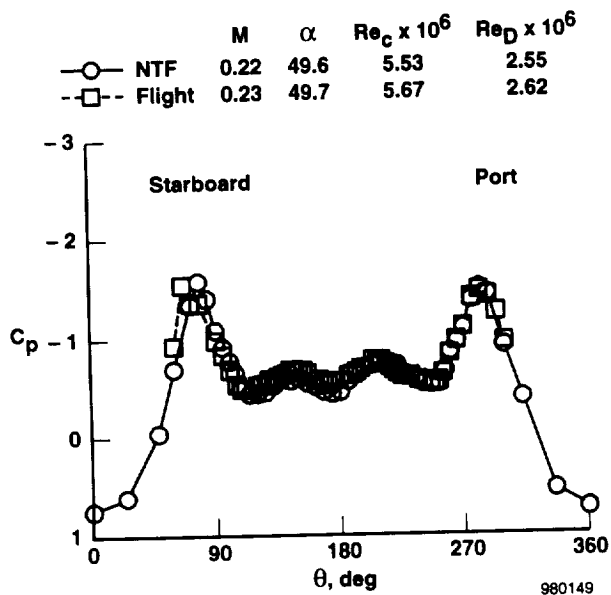
980152

Figure 32. Concluded.
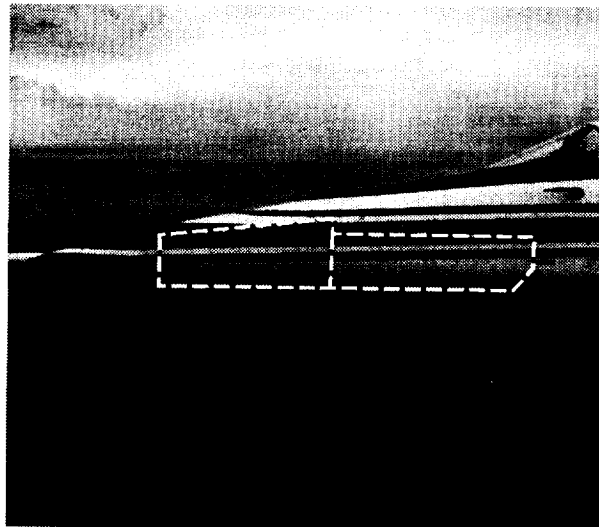
EC91-517-15

Figure 33. X-29A forebody showing access panel joints.

	M	α	q	$Re_c \times 10^6$	$Re_D \times 10^6$	Boundary layer state (Lamont's criteria)
○	0.22	66.0	74	0.68	0.31	Marginally transitional
□	0.22	65.9	200	1.90	0.87	Transitional
◇	0.22	65.9	337	3.18	1.47	Transitional
△	0.22	66.0	193	5.11	2.35	Turbulent
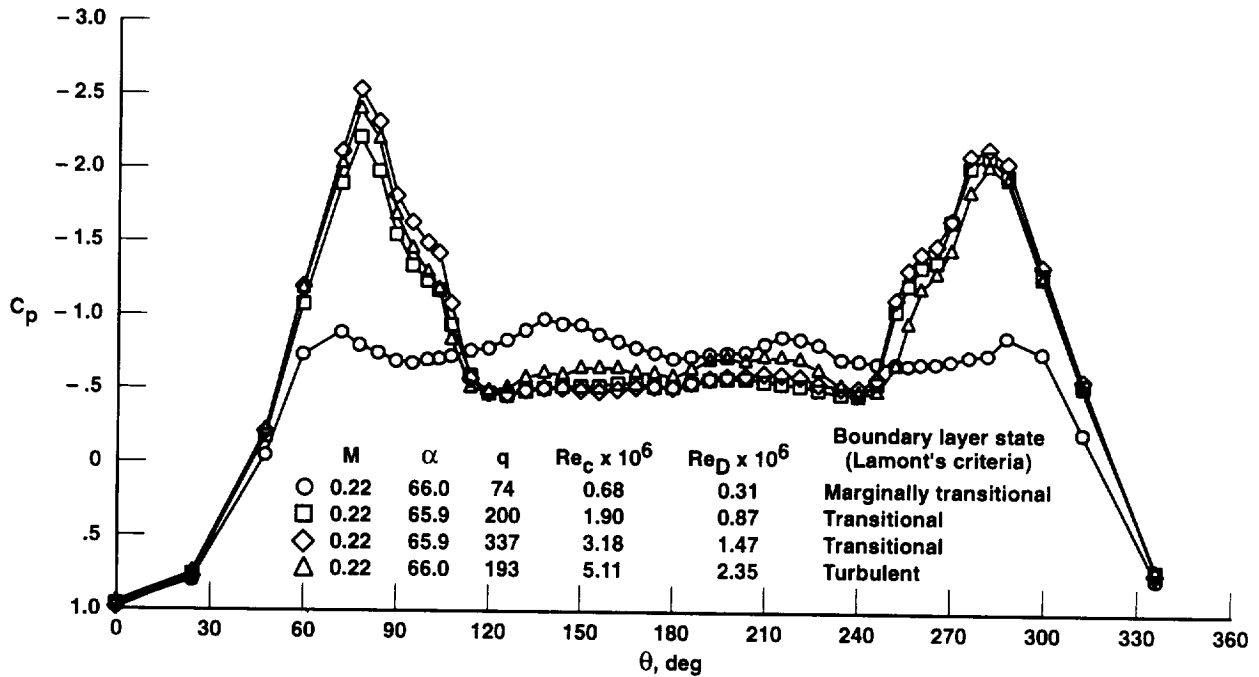
980153

Figure 34. Effect of Reynolds number on X-29 forebody pressures, $x/l = 0.136$.

27
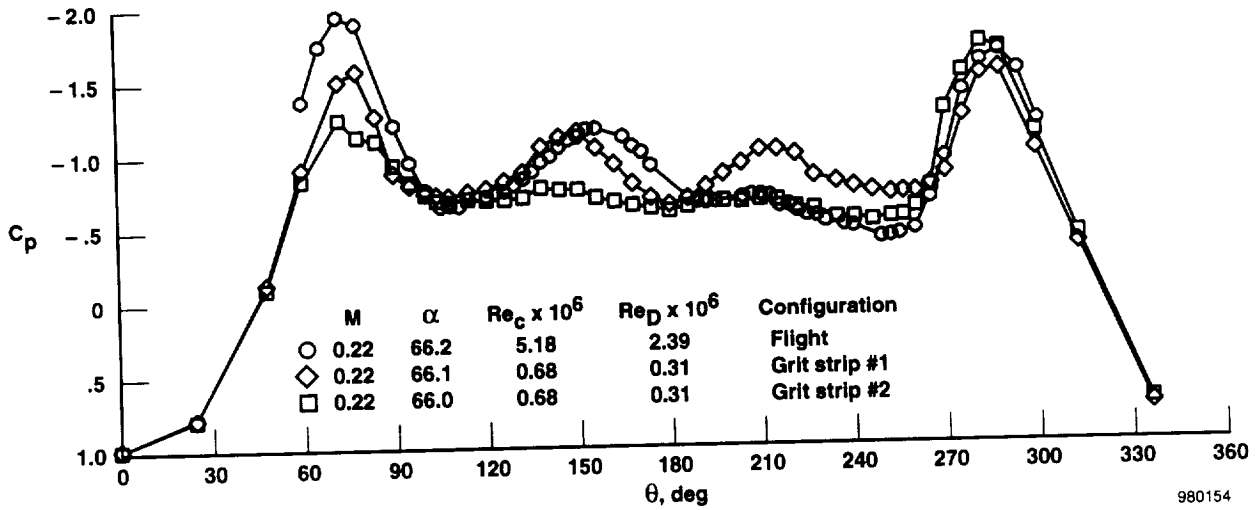
Figure 35. Correlation of X-29 forebody pressures from flight and NTF with grit strips, $x/l = 0.136$.
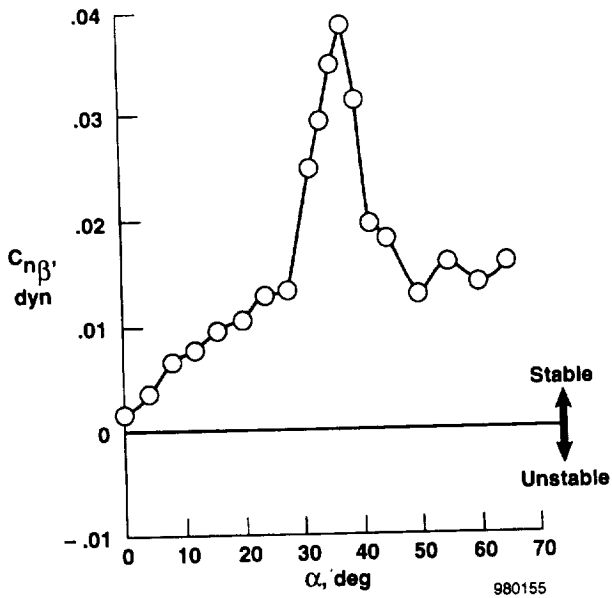
Figure 36. X-31 directional divergence parameter for trimmed configuration from wind tunnel.[27]
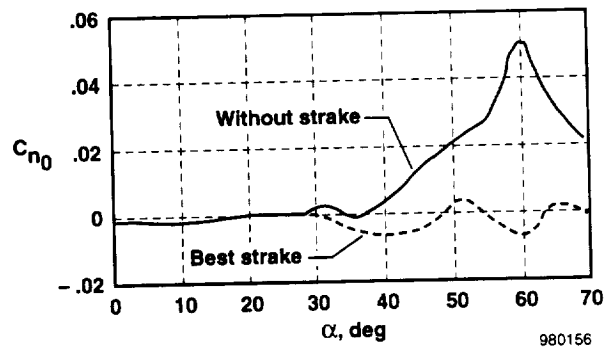
Figure 37. X-31 wind tunnel (Emmen) yawing moments with and without nose strakes, no noseboom.[28]
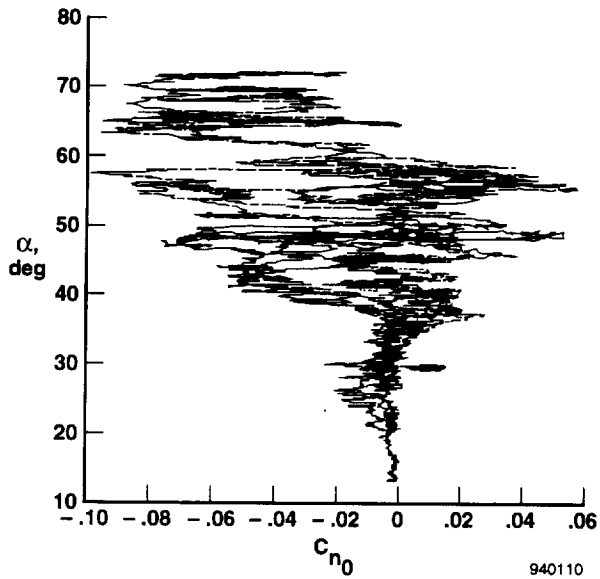
Figure 38. X-31 ship-2 asymmetry characteristics, clean configuration.[20]
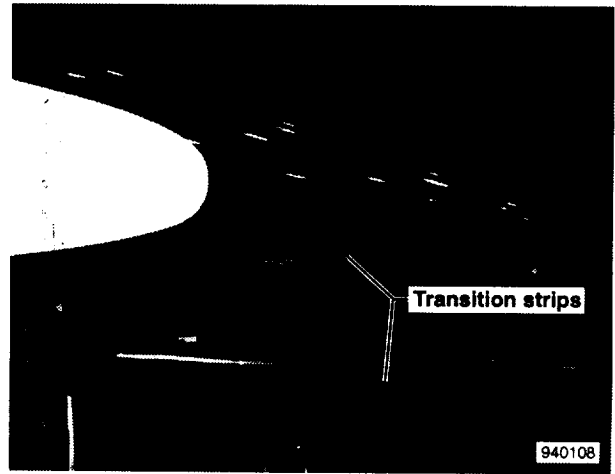
Figure 39. Grit strip on X-31 forebody and noseboom.[20]
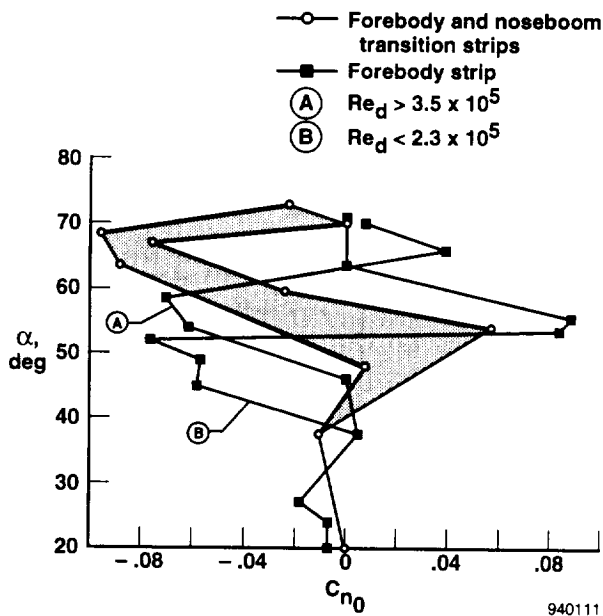
Figure 40. X-31 ship-2 asymmetry characteristics, with grit strips.[20]
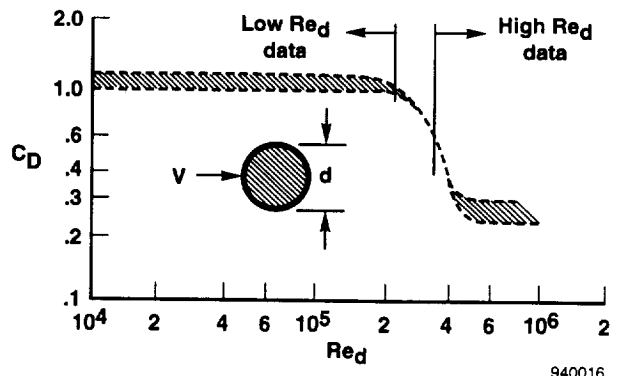
Figure 41. Variation of drag coefficient with Reynolds number for a circular cylinder.[31]

29
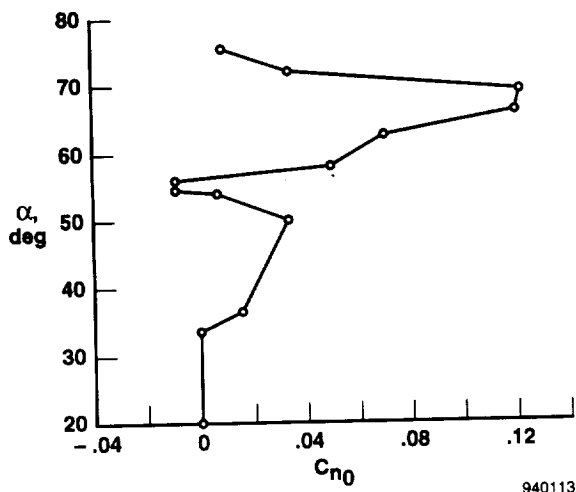
Figure 42. X-31 ship-2 yawing moment asymmetry from flight 73 departure.[20]

940113
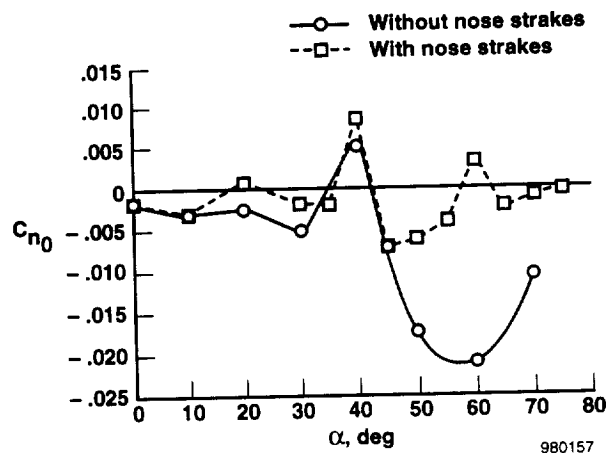
Figure 43. X-31 yawing moment with and without nose strakes, 30-by-60-Ft Wind mTunnel.[32]

980157

EC93-01061-01

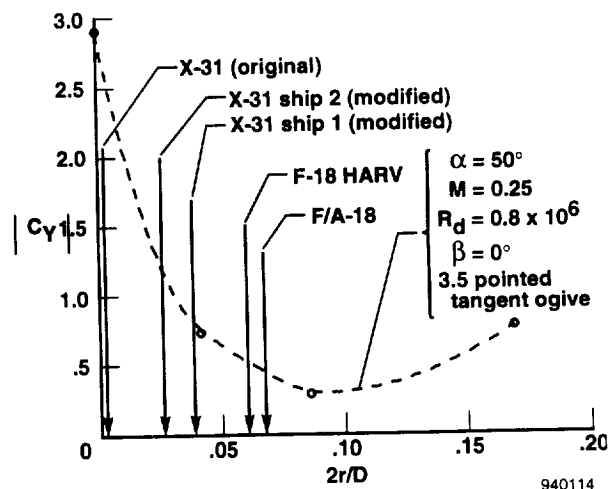Figure 44. Photograph of the 20-in. strakes installed on the X-31 forebody and rounded nosetip.[30]

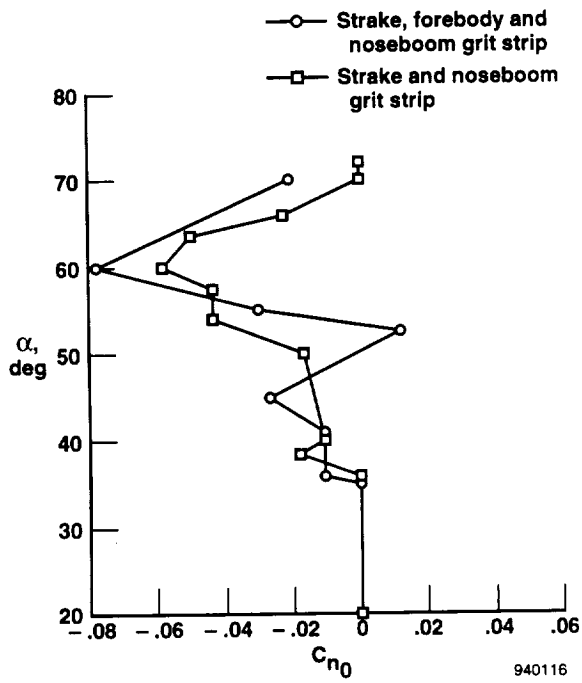Figure 45. Effect of nose bluntness on side force.[20]

940114

American Institute of Aeronautics and Astronautics

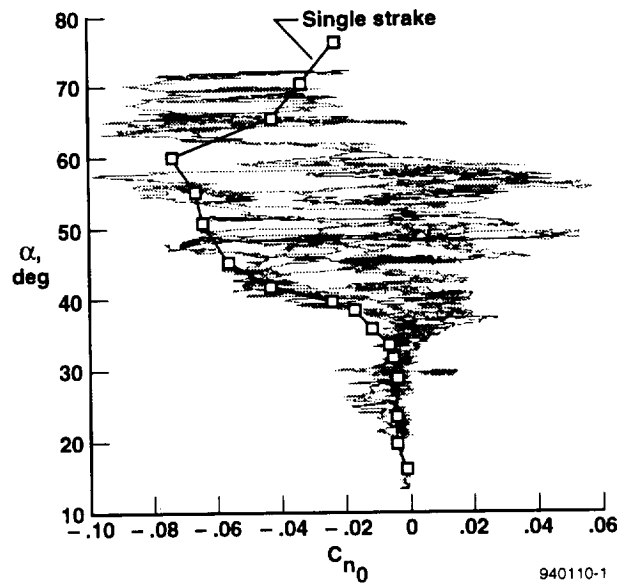Figure 46. X-31 ship-2 forebody asymmetry characteristics with forebody strakes and rounded nose.[20]

Figure 47. X-31 ship-2 asymmetry characteristics, clean configuration, compared with X-31 model with strake on one side only.[29]

REPORT DOCUMENTATION PAGE

1. AGENCY USE ONLY (Leave blank)	2. REPORT DATE	3. REPORT TYPE AND DATES COVERED
	June 1998	Technical Paper

4. TITLE AND SUBTITLE

Reynolds Number Effects at High Angles of Attack

5. FUNDING NUMBERS

WU 529-50-04-00-RR-00-000

6. AUTHOR(S)

David F. Fisher, Brent R. Cobleigh, Daniel W. Banks, Robert M. Hall, and Richard W. Wahls

7. PERFORMING ORGANIZATION NAME(S) AND ADDRESS(ES)

NASA Dryden Flight Research Center
P.O. Box 273
Edwards, California 93523-0273

8. PERFORMING ORGANIZATION REPORT NUMBER

H-2255

9. SPONSORING/MONITORING AGENCY NAME(S) AND ADDRESS(ES)

National Aeronautics and Space Administration
Washington, DC 20546-0001

10. SPONSORING/MONITORING AGENCY REPORT NUMBER

NASA/TP-1998-206553

11. SUPPLEMENTARY NOTES

Presented at 20th AIAA Advanced Measurement and Ground Testing Technology Conference, Albuquerque, New Mexico, June 15–18, 1998, AIAA-98-2879 (Invited Paper).

12a. DISTRIBUTION/AVAILABILITY STATEMENT

Unclassified—Unlimited
Subject Category 02

12b. DISTRIBUTION CODE

13. ABSTRACT (Maximum 200 words)

Lessons learned from comparisons between ground-based tests and flight measurements for the high-angle-of-attack programs on the F-18 High Alpha Research Vehicle (HARV), the X-29 forward-swept wing aircraft, and the X-31 enhanced fighter maneuverability aircraft are presented. On all three vehicles, Reynolds number effects were evident on the forebodies at high angles of attack. The correlation between flight and wind tunnel forebody pressure distributions for the F-18 HARV were improved by using twin longitudinal grit strips on the forebody of the wind-tunnel model. Pressure distributions obtained on the X-29 wind-tunnel model at flight Reynolds numbers showed excellent correlation with the flight data up to $\alpha = 50°$. Above $\alpha = 50°$ the pressure distributions for both flight and wind tunnel became asymmetric and showed poorer agreement, possibly because of the different surface finish of the model and aircraft. The detrimental effect of a very sharp nose apex was demonstrated on the X-31 aircraft. Grit strips on the forebody of the X-31 reduced the randomness but increased the magnitude of the asymmetry. Nose strakes were required to reduce the forebody yawing moment asymmetries and the grit strips on the flight test noseboom improved the aircraft

14. SUBJECT TERMS

Angle of attack, Flight test, Forebody, Noseboom, Reynolds number, Vortices, Wind tunnel

15. NUMBER OF PAGES

37

16. PRICE CODE

A03

17. SECURITY CLASSIFICATION OF REPORT	18. SECURITY CLASSIFICATION OF THIS PAGE	19. SECURITY CLASSIFICATION OF ABSTRACT	20. LIMITATION OF ABSTRACT
Unclassified	Unclassified	Unclassified	Unlimited